



## Clinical neuroanatomy

# Diffuse glioma-induced structural reorganization in close association with preexisting syntax-related networks

Ryuta Kinno <sup>a,b,\*</sup>, Yoshihiro Muragaki <sup>c</sup>, Takashi Maruyama <sup>c</sup>,  
Manabu Tamura <sup>c</sup>, Kenjiro Ono <sup>d,e</sup>, Kyohei Tanaka <sup>a</sup> and  
Kuniyoshi L. Sakai <sup>a</sup>

<sup>a</sup> Department of Basic Science, Graduate School of Arts and Sciences, The University of Tokyo, Tokyo, Japan

<sup>b</sup> Division of Neurology, Department of Internal Medicine, Showa University Northern Yokohama Hospital, Yokohama, Japan

<sup>c</sup> Department of Neurosurgery, Tokyo Women's Medical University, Tokyo, Japan

<sup>d</sup> Division of Neurology, Department of Medicine, Showa University School of Medicine, Tokyo, Japan

<sup>e</sup> Department of Neurology, Kanazawa University Graduate School of Medical Sciences, Kanazawa, Japan

## ARTICLE INFO

## Article history:

Received 27 December 2022

Reviewed 27 April 2023

Revised 16 June 2023

Accepted 14 July 2023

Action editor Cynthia Thomson

Published online 24 July 2023

## Keywords:

Fiber tracking

Glioma

Reorganization

Surface-based morphometry

Syntactic processing

## ABSTRACT

Glioma in the left frontal cortex has been reported to cause agrammatic comprehension and induce global functional connectivity alterations within the syntax-related networks. However, it remains unclear to what extent the structural reorganization is affected by preexisting syntax-related networks. We examined 28 patients with a diffuse glioma in the left hemisphere and 23 healthy participants. Syntactic abilities were assessed by a picture-sentence matching task with various sentence types. The lesion responsible for agrammatic comprehension was identified by region-of-interest-based lesion-symptom mapping (RLSM). Cortical structural alterations were examined by surface-based morphometry (SBM), in which the cortical thickness and fractal dimension were measured with three-dimensional magnetic resonance imaging (MRI). Fiber tracking on the human population-averaged diffusion MRI template was performed to examine whether the cortical structural alterations were associated with the syntax-related networks. The RLSM revealed associations between agrammatic comprehension and a glioma in the posterior limb of the left internal capsule. The SBM demonstrated that *decreased* cortical thickness and/or *increased* complexity of the right posterior insula were associated not only with agrammatic comprehension of the patients but also with the syntactic abilities of healthy participants. The fiber tracking revealed that the route between these two regions was anatomically integrated into the preexisting syntax-related networks previously identified. These results suggest a potential association between agrammatic comprehension in

\* Corresponding author. Division of Neurology, Department of Internal Medicine, Showa University Northern Yokohama Hospital, 35-1 Chigasaki-Chuo Tsuzuki-Ku, Yokohama-Shi, Kanagawa 224-8503, Japan.

E-mail address: [kinno@med.showa-u.ac.jp](mailto:kinno@med.showa-u.ac.jp) (R. Kinno).

<https://doi.org/10.1016/j.cortex.2023.07.005>

0010-9452/© 2023 The Author(s). Published by Elsevier Ltd. This is an open access article under the CC BY license (<http://creativecommons.org/licenses/by/4.0/>).

patients with diffuse glioma and structural variations in specific tracts and cortical regions, which may be closely related to the syntax-related networks.

© 2023 The Author(s). Published by Elsevier Ltd. This is an open access article under the CC BY license (<http://creativecommons.org/licenses/by/4.0/>).

### Abbreviations

Act	active sentence
Cont task	control task
DARTEL	diffeomorphic anatomical registration through the exponentiated Lie algebra
EmC	extreme capsule
FEW	family-wise error
fMRI	functional magnetic resonance imaging
FWHM	full-width half-maximum
HCP	Human Connectome Project
ILF	inferior longitudinal fasciculus
IQ	intelligence quotient
KMO	Kaiser-Meyer-Olkin
MANOVA	multivariate analysis of variance
MdLF	middle longitudinal fasciculus
MNI	Montreal Neurological Institute
Pas	passive sentence
PBT	projection-based thickness
PI	posterior insula
PLIC	posterior limb of the internal capsule
Pot	potential sentence
RLSM	region-of-interest-based lesion-symptom mapping
ROI	region-of-interest
RTs	response times
SBM	surface-based morphometry
SPH	spherical harmonics
VBM	voxel-based morphometry
VLSM	voxel-based lesion-symptom mapping

with gliomas (Duffau, 2005). Functional and structural reorganizations are thought to occur not only in the ipsilateral but also in the contralateral hemisphere (Almairac, Duffau, & Herbet, 2018; Desmurget, Bonnetblanc, & Duffau, 2007). However, it remains unclear to what extent the critical structural reorganization is affected by the preexisting networks of target functions (i.e., networks in the healthy brain), despite numerous functional neuroimaging studies that have reported global reorganizations induced by a diffuse glioma (Pasquini, Di Napoli, et al., 2022). Here, therefore, we focused on the relationships between the identified networks and the structural reorganizations induced by diffuse gliomas.

The preoperative reorganizations can explain the almost normal cognitive function of patients with diffuse gliomas under standard assessments (Desmurget et al., 2007). This poses a challenge when investigating cortical structural alterations that may be associated with cognitive abilities in these patients. Therefore, a cognitive test sensitive to the cognitive impairments of patients with diffuse gliomas is essential for elucidating the neural mechanisms of the reorganization by diffuse gliomas. We previously developed a picture-sentence matching task that was sensitive to the assessment of syntactic abilities (Fig. 1) (Kinno, Kawamura, Shioda, & Sakai, 2008). In a subsequent report, we applied this task to a voxel-based lesion-symptom mapping (VLSM) study and demonstrated that patients with a diffuse glioma in the left inferior frontal gyrus or left lateral premotor cortex showed agrammatic comprehension (Kinno et al., 2009)—i.e., deficits in understanding syntactically complex sentences but relatively good comprehension of simple sentences (Caramazza & Miceli, 1991; Schwartz, Saffran, & Marin, 1980). Furthermore, a study utilizing functional magnetic resonance imaging (fMRI) and fiber tracking identified three syntax-related networks in the healthy brain, and demonstrated the global functional connectivity alterations occurring within these networks in patients with agrammatic comprehension (Kinno, Ohta, Muragaki, Maruyama, & Sakai, 2014). Subsequent research revealed that the functional connectivity between the left frontal regions and other regions within the syntax-related networks is a key factor affecting syntactic abilities in patients with a diffuse glioma (Kinno, Ohta, Muragaki, Maruyama, & Sakai, 2015). Considering these functional connectivity alterations, we hypothesize that the diffuse glioma-induced structural reorganization for syntactic processing is closely associated with the preexisting syntax-related networks.

In the current study, we aimed to clarify the relationship between the cortical structural alterations associated with syntactic abilities and the syntax-related networks. We first examined lesions responsible for agrammatic comprehension in patients with diffuse gliomas using a lesion-symptom approach. Subsequently, we conducted surface-based morphometry (SBM) analyses to assess cortical structural

## 1. Introduction

The most frequent primary malignant brain tumors are diffuse gliomas, which are classified into grades II to IV. Gliomas in grades II and III are thought to grow slowly and be less aggressive (Motomura et al., 2019; Suzuki et al., 2015). Gliomas have various functional effects on the entire brain, including the generation of hyperexcitability throughout the brain, which can lead to epileptic attack (de Groot, Reijneveld, Aronica, & Heimans, 2012), and disruption of functional connectivity across distant regions (Bartolomei et al., 2006). These global effects include not only functional but also structural effects such as compression and infiltration to cortical regions. A recent study has demonstrated that a focal glioma causes cortical structural alterations, including changes in cortical thickness and complexity, which extend to the distant contralateral regions (Kinno et al., 2020). In addition to these global effects of gliomas, brain plasticity can also explain the alterations in brain structure and functions of patients

alterations associated with syntactic abilities. Recent advances in SBM have enabled the assessment of not only cortical thickness but also the cortical complexity of folding and gyrification. Since cortical complexity is believed to persist throughout adolescence, even subtle anomalies in complexity can be detected using appropriate techniques. The fractal dimension, which is an estimate of an object's topological complexity in general, was used to measure cortical complexity. A recent study confirmed the sensitivity of the cortical fractal dimension in detecting cortical structural alterations in patients with diffuse gliomas (Kinno et al., 2020). In the present study, therefore, we examined whether these cortical structural alterations occur within or outside previously identified syntax-related networks (Kinno et al., 2014). For this purpose, we performed fiber tracking on the healthy brain to detect fibers passing through the region responsible for agrammatic comprehension and the region with cortical structural alterations associated with syntactic abilities. Then, we compared these fibers with the preexisting syntax-

related networks. Our present findings will shed light on the principle of structural reorganizations that are closely associated with functional networks.

## 2. Materials and methods

### 2.1. Participants

The current study included 28 Japanese patients with a diffuse glioma in the left hemisphere (patient group) [16 men and 12 women, age 19–64 years; median age 39 years] (Table 1). The patients underwent preoperative structural MRI at the Komaba Campus of the University of Tokyo and glioma resection at the Department of Neurosurgery, Tokyo Women's Medical University between 2014 and 2016. Data on 15 of the patients were analyzed and reported in our previous studies (anatomical and functional study data for 9 patients (Kinno et al., 2020; Tanaka, Kinno, Muragaki, Maruyama, & Sakai,

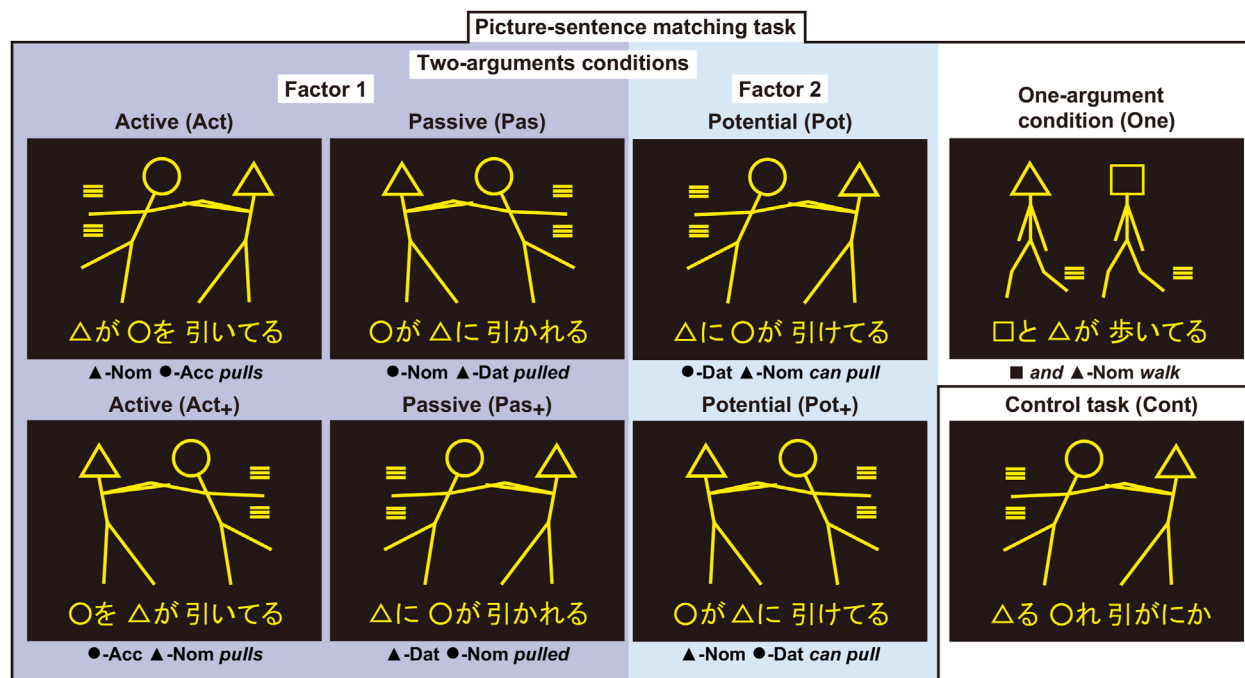


**Fig. 1** – A picture-sentence matching task and a control task. Under the two-argument (i.e., Act, Act<sub>+</sub>, Pas, Pas<sub>+</sub>, Pot, and Pot<sub>+</sub>) and one-argument (i.e., One) conditions, each stimulus consisted of one picture (top) and one sentence (bottom). The pictures consisted of two stick figures, each of which was distinguished by one of three “head” symbols: a circle, square, or triangle. For sentence stimuli, we used four kinds of grammatical particles, which represent the syntactic information in Japanese: *-ga*, a nominative (Nom) case marker; *-ni*, a dative (Dat) case marker; *-o*, an accusative (Acc) case marker; and *-to*, a coordinator (*and*). Under the two-argument conditions, we used three types of sentences as in our previous studies (Tanaka et al., 2017, 2020): active, passive, and potential sentences. The “+” symbol denotes a sentence with object scrambling. Examples of matched sentences are shown here. The English translation of each sentence is as follows: “△ pulls ○” (Act), “As for ○, △ pulls it” (Act<sub>+</sub>), “○ is affected by △’s pulling it” (Pas), “As for △’s pulling, ○ is affected” (Pas<sub>+</sub>), “△ can pull ○” (Pot), “As for ○, △ can pull it” (Pot<sub>+</sub>), and “□ and △ walk” (One). In the picture-sentence matching task, the participants read a sentence silently and judged whether or not the action depicted in a picture matched the meaning of the sentence. A factor analysis on the error rates under the two-argument conditions revealed a two-factor structure (see the Results section): a factor 1 with Act, Act<sub>+</sub>, Pas, and Pas<sub>+</sub> (in blue) and a factor 2 with Pot and Pot<sub>+</sub> (in light blue). For the Control (Cont) task, each stimulus was taken from the same sets of pictures and letters used for the picture-sentence matching task, but the letters in hiragana were jumbled without changing the head symbols and kanji. The participants judged whether or not the two head symbols in the picture matched those at the bottom, irrespective of their order.

2020); anatomical study data alone for 6 patients (Kinno et al., 2020). All 28 patients met the following criteria: (i) right handedness, (ii) no deficits in verbal/written communication or other cognitive abilities reported by the patients or physicians, (iii) no history of neurological or psychiatric disorders other than glioma and seizures, (iv) seizure-free with or without antiepileptic medications, (v) no history of brain radiotherapy, (vi) no medical problems related to MRI acquisition, (vii) no intracranial abnormalities other than glioma, and (viii) histologically proven grade II or grade III diffuse astrocytic/oligodendroglial tumors (i.e., astrocytoma, oligodendroglioma, or oligoastrocytoma) according to the 2007 WHO Classification of Tumors of the Central Nervous System (Louis et al., 2007). The Edinburgh Handedness Inventory (Oldfield, 1971) was used to calculate the laterality quotient of handedness. The intelligence quotient (IQ) was measured by the Kohs block design test.

We also recruited 23 healthy Japanese participants (control group) for both behavioral and structural MRI experiments [18 men and 5 women, age 19–55 years; median age 24 years]. There was no significant gender difference between the

patient and control groups (Fisher's exact test:  $P = .14$ ). Because the ages were considered not to be normally distributed in either group (Shapiro–Wilk test:  $P < .001$ ), we used non-parametric tests to confirm that the age difference was not significant (Mann–Whitney's  $U$ -test:  $U = 497.5$ ,  $P = .058$ ). After explaining the nature and possible consequences of the study, written informed consent was obtained from each participant. Approval for the experiment was obtained from the Institutional Review Boards of the University of Tokyo, Komaba, and Tokyo Women's Medical University.

## 2.2. Stimuli and tasks

This study used the same stimuli and task as the previous studies (Tanaka et al., 2020; Tanaka, Ohta, Kinno, & Sakai, 2017). Each visual stimulus consisted of a picture with head symbols ( $\triangle$ ,  $\circ$  or  $\square$ ) at the top, and a grammatical Japanese sentence at the bottom (Fig. 1). For each stimulus, two different head symbols were selected for a picture, and a sentence describing an action was written using a combination of the *hiragana* and *kanji* writing systems. We used four

**Table 1 – Patient characteristics.**

Patient number	LQ	IQ	Tumor location			Tumor volume	Tumor type	Tumor grade	
			x	y	z				
1	100	90	precentral gyrus	-34	4	15	137.7	AOA	III
2	100	124	insula/external capsule	-28	18	-4	53.0	AOA	III
3	68	124	insula/external capsule	-28	19	-4	109.9	AOA	III
4	65	124	middle frontal gyrus	-33	9	49	23.8	OL	II
5	86	124	inferior temporal gyrus	-40	-9	-26	54.5	AA	III
6	100	117	hippocampus	-31	-13	-22	27.9	OL	II
7	100	93	precentral gyrus	-42	1	12	81.7	AA	III
8	80	91	postcentral gyrus	-38	-16	38	98.1	AO	III
9	60	98	hippocampus	-29	-16	-24	10.3	AA	III
10	100	118	precentral gyrus	-26	-9	42	67.0	AOA	III
11	67	104	middle frontal gyrus	-37	3	41	2.1	OL	II
12	60	104	anterior corona radiata	-23	32	7	170.6	AOA	III
13	67	104	precentral gyrus	-29	-19	55	24.2	AA	III
14	100	103	postcentral gyrus	-33	-18	37	158.7	OL	II
15	63	117	superior temporal gyrus	-43	-7	-10	126.3	AA	III
16	100	124	pars opercularis	-41	9	6	22.2	AA	III
17	100	93	superior temporal gyrus	-52	-36	12	29.9	AOA	III
18	89	122	supramarginal gyrus	-49	-35	34	29.9	AOA	III
19	100	124	middle temporal gyrus	-56	-33	-11	7.5	OL	II
20	100	124	superior frontal gyrus	-16	17	45	119.7	OL	II
21	80	109	anterior corona radiata	-25	35	6	145.9	AO	III
22	78	109	pars opercularis	-43	9	9	33.7	OL	II
23	80	91	superior temporal gyrus	-46	-17	1	44.6	AO	III
24	100	124	precentral gyrus	-50	5	7	13.9	DA	II
25	100	124	middle frontal gyrus	-27	45	12	21.9	DA	II
26	87	118	inferior fronto-occipital fasciculus	-24	10	-10	55.3	AA	III
27	100	116	middle frontal gyrus	-26	-5	52	42.5	AA	III
28	100	124	pars triangularis	-30	26	-8	11.2	OL	II
Mean	86.8	112.0							

The laterality quotient of handedness was determined by the Edinburgh Handedness Inventory (Oldfield, 1971). MR images were normalized with SPM12 to determine the tumor location (the center of geometry), as well as the tumor volume ( $\text{cm}^3$ ) of a tumor, including the gray matter and white matter. The determination of tumor types and grades (II or III, with III being more severe) was based on the 2007 WHO Classification of Tumors of the Central Nervous System (Louis et al., 2007). The method of determining tumor locations was previously described (Kinno et al., 2014). MNI coordinates of each tumor location (the center of geometry) and its location are shown. AA = anaplastic astrocytoma (grade III), AO = anaplastic oligodendroglioma (grade III), AOA = anaplastic oligoastrocytoma (grade III), DA = diffuse astrocytoma (grade II), IQ = intelligence quotient (measured by the Kohs block design test), LQ = laterality quotient, OA = oligoastrocytoma (grade II), OL = oligodendroglioma (grade II).

different types of Japanese grammatical particles, which represent the syntactic information: *-ga*, *-ni*, *-o*, and *-to* [a coordinator (and)].

We tested two types of conditions with different sets of stimuli: two-argument and one-argument conditions. Under the two-argument conditions with an identical picture set, we tested six different sentence types (Fig. 1): active (Act) (e.g., “*△-ga* ○-*o* *hiiteru*,” or “*△* pulls ○” in English), passive (Pas) (e.g., “○-*ga* *△-ni* *hikareru*,” or “○ is affected by *△*’s pulling it”), and potential (Pot) (e.g., “*△-ni* ○-*ga* *hiketeru*,” or “*△* can push ○”) sentences, as well as scrambled active (e.g., “○-*o* *△-ga* *hiiteru*,” or “As for ○, *△* pulls it”), scrambled passive (e.g., “*△-ni* ○-*ga* *hikareru*,” or “As for ○’s pulling, *△* is affected”), and scrambled potential (e.g., “○-*ga* *△-ni* *hiketeru*,” or “As for ○, *△* can push it”) sentences. Here, the term “scrambling” refers to the syntactic operation of moving an object to the initial position of a sentence for the purpose of emphasizing it. Hereinafter we use the term “object scrambling” to refer to this type of syntactic movement. Japanese is a subject-object-verb language with a flexible word order, which means that the word order of scrambled sentences is noncanonical but perfectly grammatical in Japanese. The sentences with scrambling are marked here with the symbol “+”, as in Act+, Pas+, and Pot+. Under the one-argument condition, each sentence was a double-subject (double-agent) type and ended with an intransitive verb (e.g., “□-*to* *△-ga* *aruiteru*,” or “□ and *△* walk”). We did not use the topic marker “-*wa*” for the subject to control for the effect of topicalization. This is because in Japanese, replacing the nominative marker “-*ga*” with the topic marker “-*wa*” induces the effects of topicalization in addition to those of object scrambling (Imamura, Sato, & Koizumi, 2016; Ohta, Koizumi, & Sakai, 2017).

In the picture-sentence matching task, the participants were asked to read a sentence silently and judge whether the actions depicted in the picture matched the meaning of the sentence. They were instructed to respond by pressing one of two buttons. The stimulus presentation and collection of behavioral data [error rates and response times (RTs)] were controlled using the LabVIEW software and interface (National Instruments, Austin, TX). For the Control (Cont) task, using the same stimulus sets of pictures and letters presented under the conditions described above, the participants judged whether or not the two head symbols in the picture matched those at the bottom, regardless of their order. The position of the letters in hiragana were jumbled without changing that of the head symbols and kanji, so that the letter string prevented even basic word recognition. Each stimulus was presented for 6 sec (fixed intratrial interval) followed by a 2-sec blank interval. A single scanning run (256 sec) contained 32 trial events (4 for each of the Act, Act+, Pas, Pas+, Pot, Pot+, one-argument, and Cont task conditions), the order of which was pseudorandomized to prevent any condition-specific strategy. Six runs were administered, and the participants did not encounter the same sentence twice.

### 2.3. Exploratory factor analysis

Behavioral data on both patient and control groups were analyzed by an exploratory factor analysis using JMP-pro (version 16.0.0; SAS Institute Inc., Cary, NC, USA).

Exploratory factor analysis is generally used when the sample size is large, but it has also been shown to yield reliable results with sample sizes considerably lower than 50 (de Winter, Dodou, & Wieringa, 2009; Sapnas & Zeller, 2002). Our sample size was  $n = 51$ , acceptable for an exploratory factor analysis, and our analysis was based on the correlation matrix of the error rates (Table 2) under the two-argument conditions (Act, Act+, Pas, Pas+, Pot, and Pot+). To assess the suitability of our data for an exploratory factor analysis, we first checked the Kaiser-Meyer-Olkin (KMO) test and Bartlett’s Test for Sphericity (Bartlett, 1950; Kaiser & Rice, 1974). The KMO test is a measure of the proportion of variance among variables that might account for common variance; a KMO value of more than .6 indicates that the correlation matrix is adequate (Howard, 2016). Bartlett’s Test of Sphericity tests the null hypothesis that the correlation matrix is an identity matrix, where variables (i.e., error rates here) are unrelated and thus unsuitable for a meaningful analysis. The correlation matrix under the two argument conditions was suitable for an exploratory factor analysis, because the KMO value was .77, and Bartlett’s Test of Sphericity was significant [ $\chi^2(15) = 168.12, P < .001$ ]. We used a maximum likelihood estimation with promax rotation, and the number of factors was identified by the Kaiser criterion (eigenvalue  $>1.00$ ), where factor loadings greater than .60 were considered significant. Finally, we estimated factor scores for the following neuroimaging analyses. To obtain the factor scores, the standardized error rates for a condition were weighted (multiplied) with their factor loadings for each factor (factor 1 or factor 2), and the resultant data were summed up. This means that the participants with higher factor scores performed worse under the conditions associated with that factor.

### 2.4. MRI data acquisition and processing

A 3.0 T system (GE Signa HDxt 3.0 T; GE Healthcare, Milwaukee, WI, USA) was used for the MRI scans. We obtained high-resolution T1-weighted images of the whole brain (136 axial slices,  $1.0 \times 1.0 \times 1.0 \text{ mm}^3$ ) from all participants with a three-dimensional fast spoiled gradient recalled acquisition in the steady state sequence (repetition time = 8.4 ms, echo time = 2.6 ms, flip angle =  $25^\circ$ , field of view =  $256 \times 256 \text{ mm}^2$ ). The structural MRI data preprocessing was performed using the CAT12 Toolbox (Structural Brain Mapping Group, Jena University Hospital, Jena, Germany; <http://dbm.neuro.uni->

**Table 2 – Inter-correlation matrix for the picture-sentence matching task.**

	Error rates					
	Act	Act+	Pas	Pas+	Pot	Pot+
Act						
Act+	.66*					
Pas	.81*	.77*				
Pas+	.62*	.75*	.76*			
Pot	.10	.24	.20	.38		
Pot+	.12	.27	.11	.27	.50*	

Pearson’s  $r$  values are shown for the error rates of all participants. The asterisks indicate significant correlations at  $P < .05$ .

[jena.de/cat/](http://jena.de/cat/)) included in the SPM12 statistical parametric mapping software (Wellcome Trust Centre for Neuroimaging; <http://www.fil.ion.ucl.ac.uk/spm/>) (Friston et al., 1995), and implemented in MATLAB software (MathWorks, Natick, MA, USA). The T1-weighted anatomical images were normalized to the Montreal Neurological Institute (MNI) space and segmented into grey matter, white matter, and cerebrospinal fluid using the default settings of the CAT 12 Toolbox. We used the East Asian brain template for affine registration. Next, the images were normalized to the MNI space by using a diffeomorphic non-linear registration algorithm of the diffeomorphic anatomical registration through the exponentiated Lie algebra (DARTTEL) toolbox (Ashburner, 2007). The final resulting voxel size was  $1.5 \times 1.5 \times 1.5 \text{ mm}^3$ . All of the resulting images were visually checked for the absence of artifacts. They also passed the quality and homogeneity checking algorithms implemented in the CAT12 Toolbox. The normalized T1-weighted anatomical images were then used to determine the tumor location for each patient.

## 2.5. Lesion analyses

The lesions analyses were performed using the same procedures as in previous studies (Kinno et al., 2020; Tanaka et al., 2020). Each glioma was detected by expert neurologists and neurosurgeons on normalized T1-weighted structural images, and the glioma boundary was semi-automatically determined using the 3D Fill tool in the MRICroGL software package (University of South Carolina, Columbia, SC, USA; <https://www.nitrc.org/projects/mricrogl/>), which generated a contiguous cluster of voxels defined by the intensity of the glioma itself. The boundaries of each lesion, including brain edemas and perfusion abnormalities, were confirmed with the T2-weighted MR images taken at the Department of Neurosurgery. The absence of skip lesions distant from the glioma was confirmed with  $^{11}\text{C}$ -methionine,  $^{18}\text{F}$  fluorodeoxyglucose, and  $^{11}\text{C}$ -choline PET data (resolution =  $4.8 \times 4.8 \times 4.25 \text{ mm}^3$ ) taken at the Chubu Medical Center for Prolonged Traumatic Brain Dysfunction (Minokamo City, Gifu, Japan). Lesion overlap maps were computed with the MRICroGL software, then converted to the standard surface template and visualized with the CAT12 Toolbox. The center of geometry for each tumor was calculated with MRICroGL software. We estimated the volume and center of geometry for each tumor on the normalized T1-weighted image. The axial slices at the level of the midbrain ( $z = 10$ ) and the body of the corpus callosum ( $z = 35$ ) confirmed that none of the patients' normalized MR images had any visible midline shift.

The lesion overlap map (Fig. 2A) showed that the patients had a diffuse glioma mainly in the left perisylvian regions, including the inferior frontal gyrus, superior temporal gyrus, and middle temporal gyrus. The second-largest overlap lesion was in the left middle frontal gyrus. On the axial sections of the lesion overlap map (Fig. 2B), overlapped lesions in the left frontal gyrus extending into the left insula and internal capsule were observed. According to Spearman's rank correlation tests, the tumor location (i.e., the MNI coordinates for the center of geometry) was not significantly affected by the tumor volume ( $x$ -,  $y$ -, and  $z$ -axis: all,  $P > .36$ ), laterality quotient (all,  $P > .69$ ), or

age (all,  $P > .49$ ). Mann–Whitney's  $U$  tests showed that gender did not significantly influence the tumor location (all,  $P > .27$ ). Therefore, the subsequent effects revealed by neuroimaging analyses (Figs. 3–7) were due to the presence of a randomly localized glioma in the left hemisphere.

## 2.6. Regions of interest-based lesion-symptom mapping

Using individually normalized images, we then performed region-of-interest (ROI)-based lesion-symptom mapping (RLSM) to analyze the relationship between glioma location and the factor scores from the exploratory factor analysis. The RLSM analysis was performed by using NiiStat scripts (University of South Carolina, Columbia, SC, USA; <http://www.nitrc.org/projects/niistat/>) implemented in MATLAB software. In the RLSM analysis, segmentation was performed according to the Johns Hopkins University (JHU) neuroanatomical atlas that segments the brain into 189 regions (Faria et al., 2012). Patients were divided into two groups according to the presence or absence of diffuse gliomas in each divided region. To minimize the impacts of outlier observations, the ROIs used in the RLSM analysis were within the glioma for at least 10% (i.e., 3) of the patients tested. The factor scores were then compared between these two groups by a  $t$ -test, and the resultant map was projected onto the axial slices of the standard brain. The statistical threshold was set to  $P = .05$  after Bonferroni correction. Finally, the results of RLSM were projected onto a standard brain using MRICroGL software.

## 2.7. Surface-based morphometry

SBM analysis was performed by using the CAT12 Toolbox under the default settings, basically as described in our previous study (Kinno et al., 2020). In brief, the cortical surface extraction from the T1-weighted MR images, as well as the estimation of cortical thickness, was performed by a projection-based thickness (PBT) approach (Dahnke, Yotter, & Gaser, 2013). A topology correction based on spherical harmonics (SPH) was used to correct the topology of the cortical surface generated with the PBT approach (R. A. Yotter, Dahnke, Thompson, & Gaser, 2011). A fast algorithm was used to reduce the area distortion of the input spherical map, leading to an improved reparameterization of the surface mesh (R. A. Yotter, Thompson, & Gaser, 2011). For the spherical registration, an adapted two-dimensional diffeomorphic DARTTEL algorithm (Ashburner, 2007) was then applied to the surface. In addition, the fractal dimension values were calculated by using SPH expansions (Nenadic, Yotter, Sauer, & Gaser, 2014; R. A. Yotter, Nenadic, Ziegler, Thompson, & Gaser, 2011; Rachel Aine Yotter, Thompson, Nenadic, & Gaser, 2010). For inter-participant analyses, the cortical thickness and fractal dimension maps from each participant were re-parameterized into a common coordinate system. This was accomplished by using the registered spherical meshes (*rh.sphere.reg* and *lh.sphere.reg*), followed by mapping to the standard template [the surface mesh of *fsaverage* (average subject)]. Finally, all data were smoothed with a Gaussian kernel of 20 mm full-width half-maximum (FWHM).

For the SBM analysis, we tested the association between variables (factor scores or the volume of a diffuse glioma in the posterior limb of the internal capsule (PLIC)) and cortical parameters (cortical thickness or fractal dimension) using multiple regressions analyses within each group. Statistical analyses were performed using the general linear model approach implemented in SPM12. Cortical structures are known to be affected by gender and age (Luders et al., 2006; Salat et al., 2004), and we thus included gender and age as nuisance factors in the design matrix of SBM analysis. The surface data were thresholded at uncorrected  $P < .001$  for the

vertex level, and at corrected  $P < .05$  for the cluster level, with family-wise error (FWE) correction across the whole brain. Using the CAT12 Toolbox, the anatomical location of a diffuse glioma or cluster was determined with reference to the multi-modal analyses of MR images from the Human Connectome Project (HCP) (Glasser et al., 2016).

## 2.8. Fiber tracking

To examine the anatomical connections in the healthy brain, we performed fiber tracking on the human population-

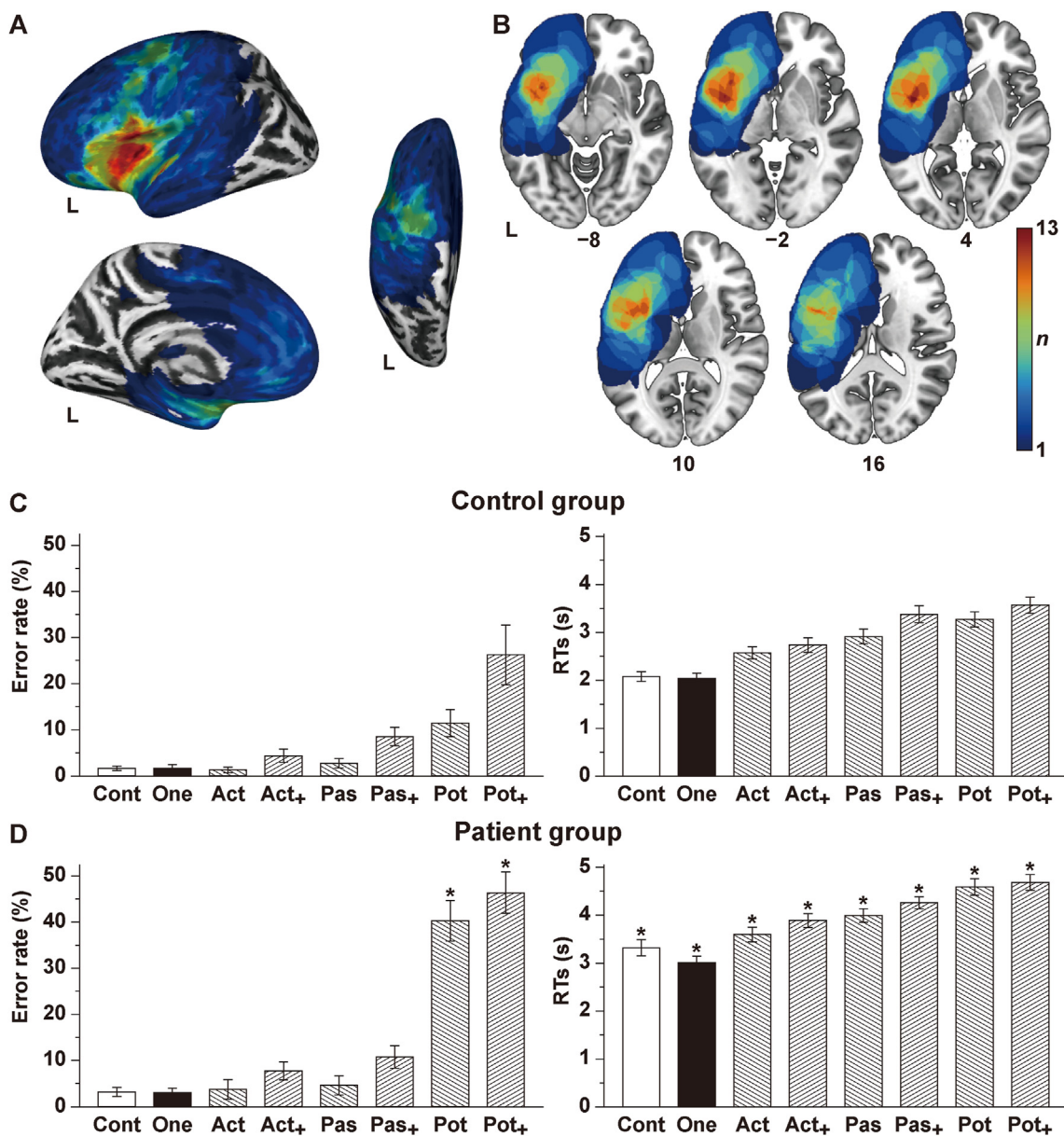


**Fig. 2 – Lesion overlap maps and behavioral data. (A, B)** Lesion overlap maps for the patient group. For the left (L) hemisphere of the inflated standard brain, the lateral (left top), medial (left bottom), and dorsal (right) views (A) are shown. Lesion overlap maps projected onto the axial slices (B) are also shown. The color bar denotes the number of patients. (C, D) Histograms of error rates and response times (RTs) for the control (C) and patient groups (D). Error bars indicate the standard error of the mean. An asterisk just above a bar for the patient group denotes error rates significantly higher than those under the same condition for the control group ( $*P < .05$ , t-test). Act = active; Act<sub>+</sub> = scrambled active; Cont = control task; One = one-argument; Pas = passive, Pas<sub>+</sub> = scrambled passive; Pot = potential; Pot<sub>+</sub> = scrambled potential.

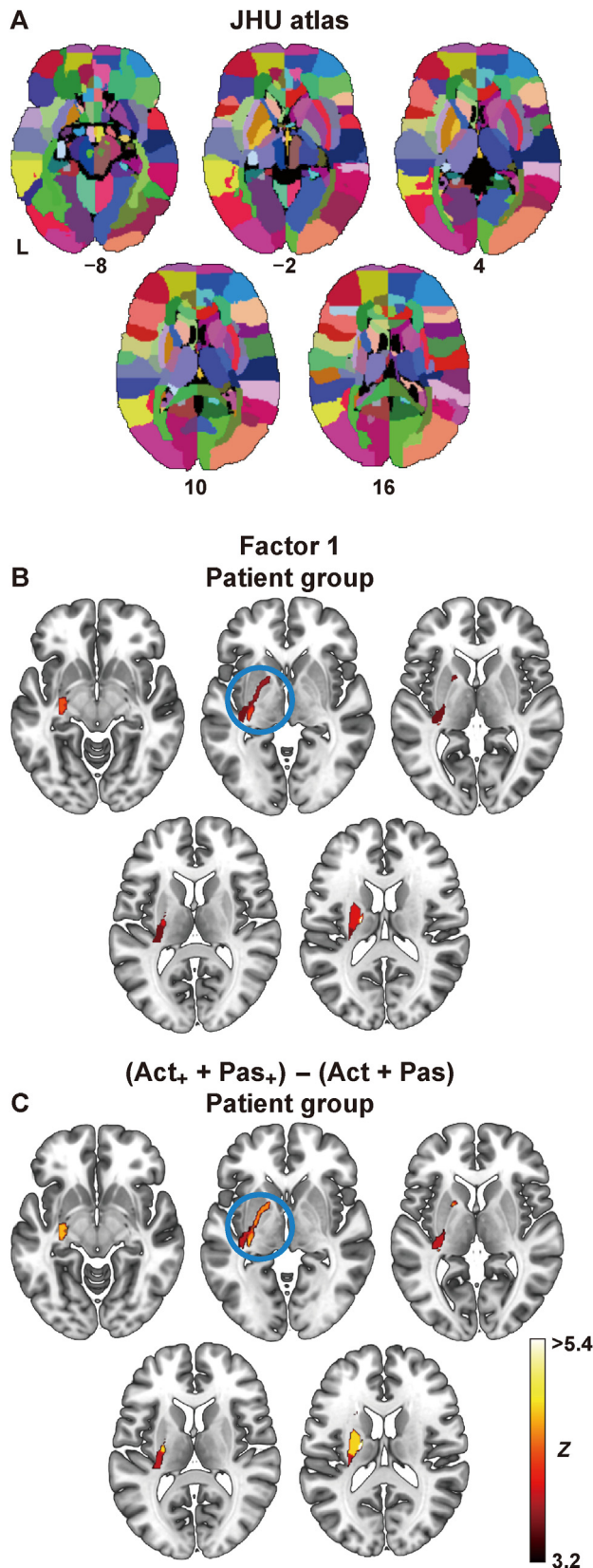


**Fig. 3** – Lesion responsible for agrammatic comprehension. (A) The Johns Hopkins University (JHU) atlas (cited from Faria et al., 2012) was used in the ROI-based lesion-symptom mapping (RLSM). (B) RLSM for the factor 1 scores. In the RLSM analysis, the lesion data of

averaged diffusion MRI template of HCP-842, which was constructed from the diffusion MRI data of 842 healthy participants in the HCP Project (Yeh et al., 2018) ([https://brain.labsolver.org/hcp\\_template.html](https://brain.labsolver.org/hcp_template.html)). For this template, a multi-shell diffusion MRI with the  $b$ -values of 990, 1985, and 2980  $\text{sec}/\text{mm}^2$  was acquired from each participant, where the number of diffusion sampling directions was 90 for each axis (spatial resolution:  $1.25 \times 1.25 \times 1.25 \text{ mm}^3$ ). The diffusion data were reconstructed into the MNI space using the generalized Q-sampling imaging approach (Yeh, Wedeen, & Tseng, 2010). A diffusion sampling length ratio of 1.25 was used, and the output resolution was 2 mm. We employed a deterministic fiber tracking algorithm using DSI studio software (University of Pittsburgh, Pittsburgh, PA, USA; <http://dsi-studio.labsolver.org/>) (Yeh, Verstynen, Wang, Fernandez-Miranda, & Tseng, 2013). In the present study, a seeding region was placed at the white matter, and we randomly selected the tracking parameters, including the anisotropy threshold, angular threshold, and step size, using a random generator to saturate the parameter space. This approach can explore millions of parameter combinations to maximize the mapping of fiber pathways, which improves the test-retest reliability of analyses and makes the results robust to different parameter settings (Yeh, 2020). The anisotropy threshold was randomly selected within the range of .5–.7 of the Otsu's threshold, whereas the angular threshold was randomly selected within the range of  $15$ – $90^\circ$ . The step size was randomly selected within the range of .5–1.5 voxels. Tracks with length shorter than 30 mm or longer than 300 mm were discarded. The fiber trajectories were smoothed by averaging the propagation direction with 20% of the previous direction. The tracking stopped when we calculated a total of 5000 tracts that passed through both of the selected ROIs.

We selected the ROIs for the fiber tracking as follows. The ROI of the left PLIC was identified by using the RLSM-generated image. The ROI of the right posterior insula (PI) was created based on the HCP-MMP atlas (Glasser et al., 2016). The ROIs for the 14 syntax-related regions were created using the “assign a sphere region” option in the DSI studio, where a sphere of 6-mm radius centered at the coordinates derived from our previous study (Kinno et al., 2014) was defined as a ROI.

each patient were segmented according to the JHU atlas, and then the patients were divided into two groups according to whether they did or did not have a diffuse glioma that involved that segmented area. The factor scores were then compared for these two groups by a  $t$ -test, and the resultant map was projected onto the axial slices of the standard brain. The color bar denotes significant  $Z$ -values in the ROIs (Bonferroni-corrected  $P < .05$ ), which represent increases in the factor 1 scores (i.e., higher error rates of Act, Act<sub>+</sub>, Pas, and Pas<sub>+</sub>) for the patient group with a diffuse glioma in the ROI. The statistical values were assigned for each ROI. (C) RLSM for the differences in the error rates  $[(\text{Act}_+ + \text{Pas}_+) - (\text{Act} + \text{Pas})]$ . Note the significantly increased factor 1 scores as well as the significantly larger differences in the error rates  $[(\text{Act}_+ + \text{Pas}_+) - (\text{Act} + \text{Pas})]$  for the patients with a diffuse glioma in the left PLIC (blue circles).

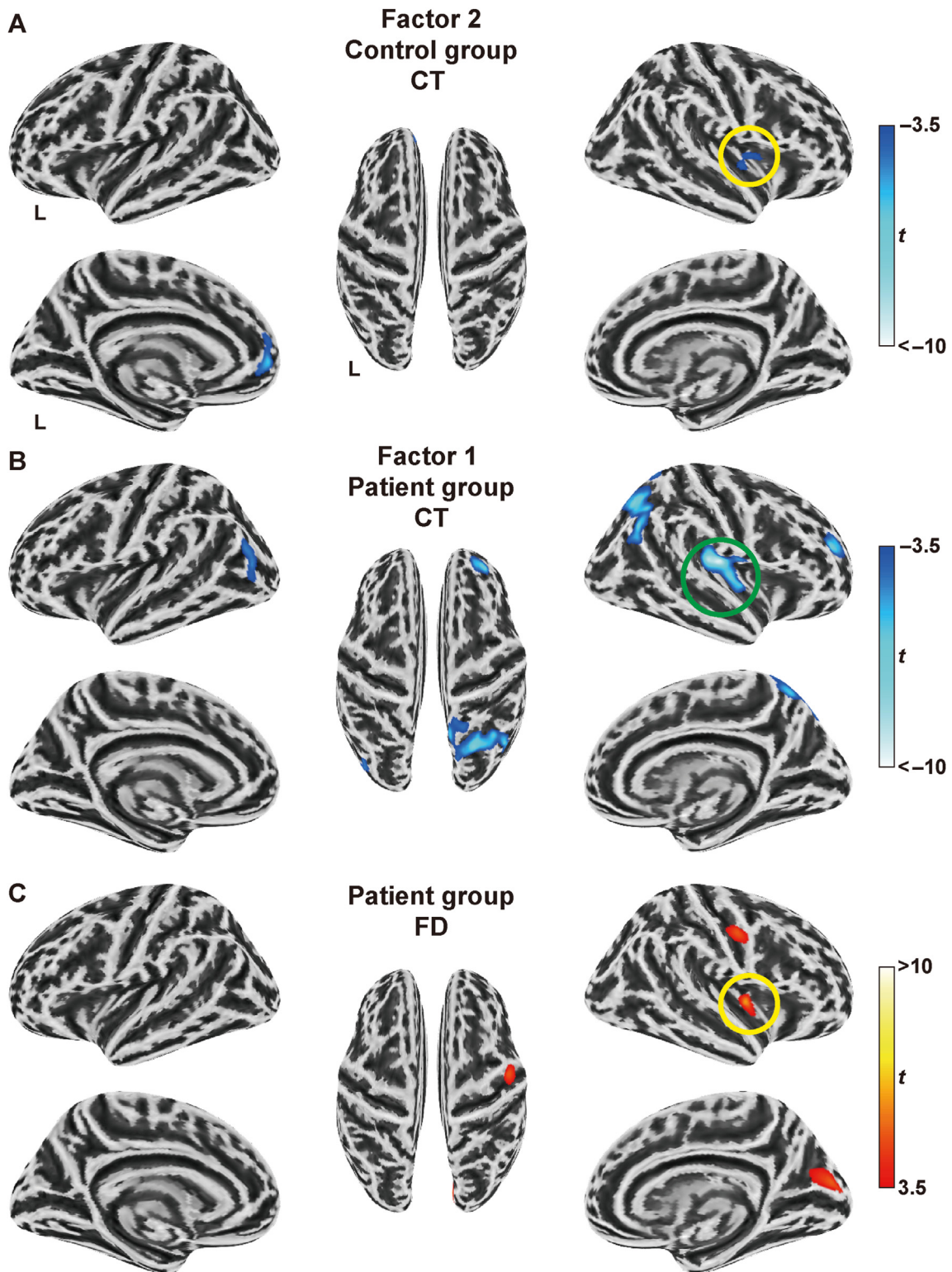
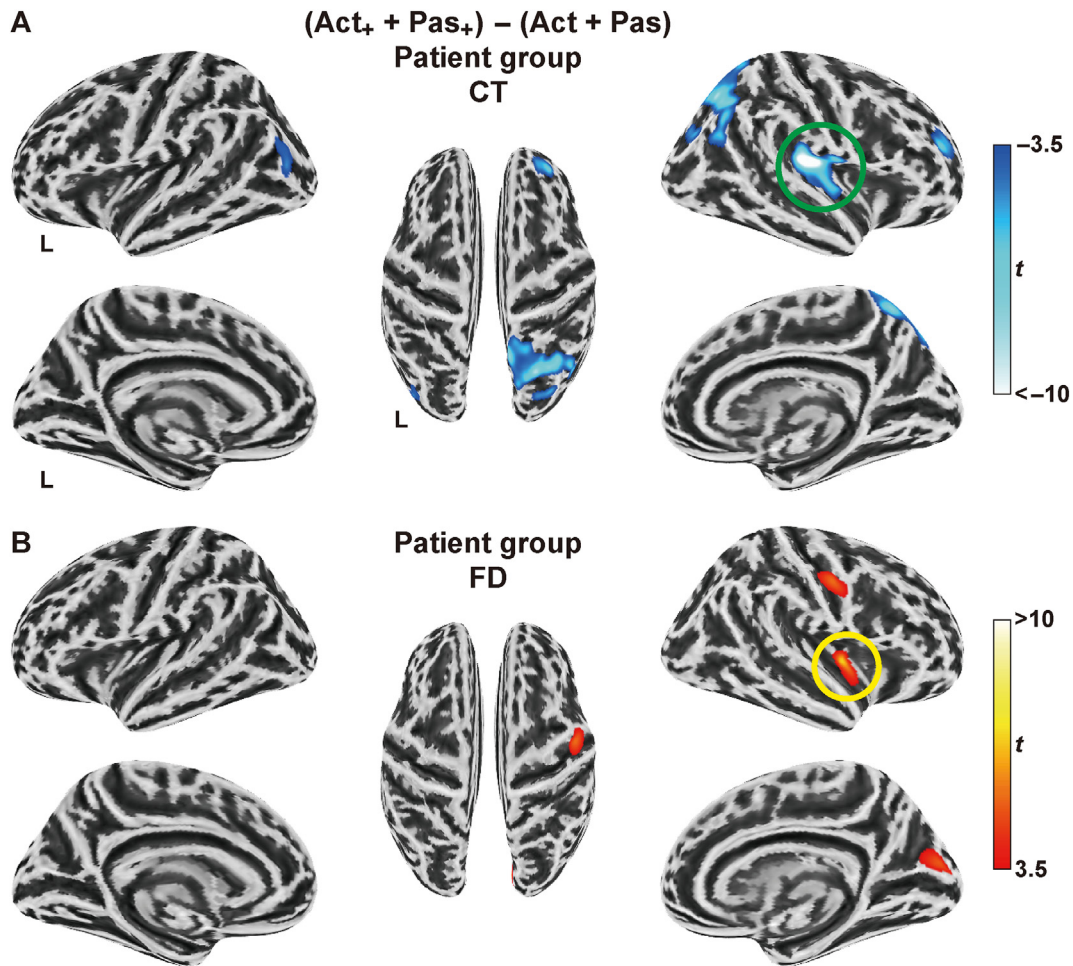


Fig. 4 – Cortical structural alterations associated with the factor scores. (A) Brain regions with significantly decreased cortical thickness (CT), which were associated with the factor 2 score for the control group. These regions were projected onto the inflated standard brain (FWE-corrected  $P < .05$  at the cluster level). Lateral (left top and right top), medial (left bottom and right bottom), and dorsal (center) views of both hemispheres are shown (the same configuration for subsequent panels). The color bar denotes the t-values of each region. Note the significant region of the right posterior insula (PI) (yellow circle). (B, C) Brain regions with significantly decreased cortical thickness (B) and increased fractal dimension (C), which were associated with the factor 1 scores for the patient group. The right PI was identified by the SBM for cortical thickness (green circle) and fractal dimension (yellow circle). Note the spatial consistency of the right PI for the control (A) and patient (C) groups (yellow circles).



**Fig. 5** – Cortical structural alterations associated with the object scrambling effects. (A, B) Brain regions with significantly decreased cortical thickness (A) and increased fractal dimension (B), which were associated with larger differences in the error rates [(Act<sub>+</sub> + Pas<sub>+</sub>) – (Act + Pas)]. The right PI was identified by the SBM for cortical thickness (green circle) and fractal dimension (yellow circle). Note the spatial consistency of the right PI for the factor score (Fig. 4) and these analyses.

### 3. Results

The presentation of results is organized as follows. We first analyzed the behavioral data (Fig. 2C and D) and extracted major factors reflecting the condition-specific effects under the two-argument conditions (Tables 2 and 3). Next, we performed the RLSM and SBM analyses to identify any regions exhibiting the cortical structural alterations associated with these factors (Figs. 3–5). We then examined the relationships between the region identified in the RLSM and that in the SBM (Fig. 6). Finally, we used fiber tracking to clarify the anatomical connections between these regions and compared them with the previously identified syntax-related networks (Fig. 7).

#### 3.1. Condition-specific effects associated with syntactic abilities

Error rates and RTs are shown in Fig. 2C and D. Under the Pas<sub>+</sub>, Pot, and Pot<sub>+</sub> conditions, not only the patients but also the controls showed higher error rates and longer RTs compared

with those under the other conditions. Because the effect of general cognitive demands was identical among the tested conditions (see Fig. 1), this trend would have been due to the condition-specific effects reflecting syntactic loads for both groups. To examine such effects under the two-argument conditions, we first performed a repeated measures multivariate ANOVA (MANOVA) with two factors [group (patient, control) × condition (Act, Act<sub>+</sub>, Pas, Pas<sub>+</sub>, Pot, Pot<sub>+</sub>)]. Mauchly's test indicated that the assumption of sphericity had been violated for the main effect of condition [error rates:  $\chi^2(14) = 234.41, P < .001$ ; RTs:  $\chi^2(14) = 68.23, P < .001$ ]. Therefore, the degrees of freedom were corrected with the Greenhouse-Geisser estimates of sphericity (error rates:  $\epsilon = .41$ ; RTs:  $\epsilon = .60$ ). A repeated measures MANOVA on the error rates revealed significant main effects of group [F (1, 49) = 13.23,  $P < .001$ ] and condition [F (2.06, 101.07) = 51.73,  $P < .001$ ], as well as a significant interaction between them [F (2.06, 101.07) = 9.25,  $P < .001$ ]. When compared with the control group, the patient group (Fig. 2D) showed significantly higher error rates under the Pot (two-sample t-tests,  $t(49) = 5.2, P < .001$ ) and Pot<sub>+</sub> ( $t(49) = 2.6, P = .012$ ) conditions. In contrast,

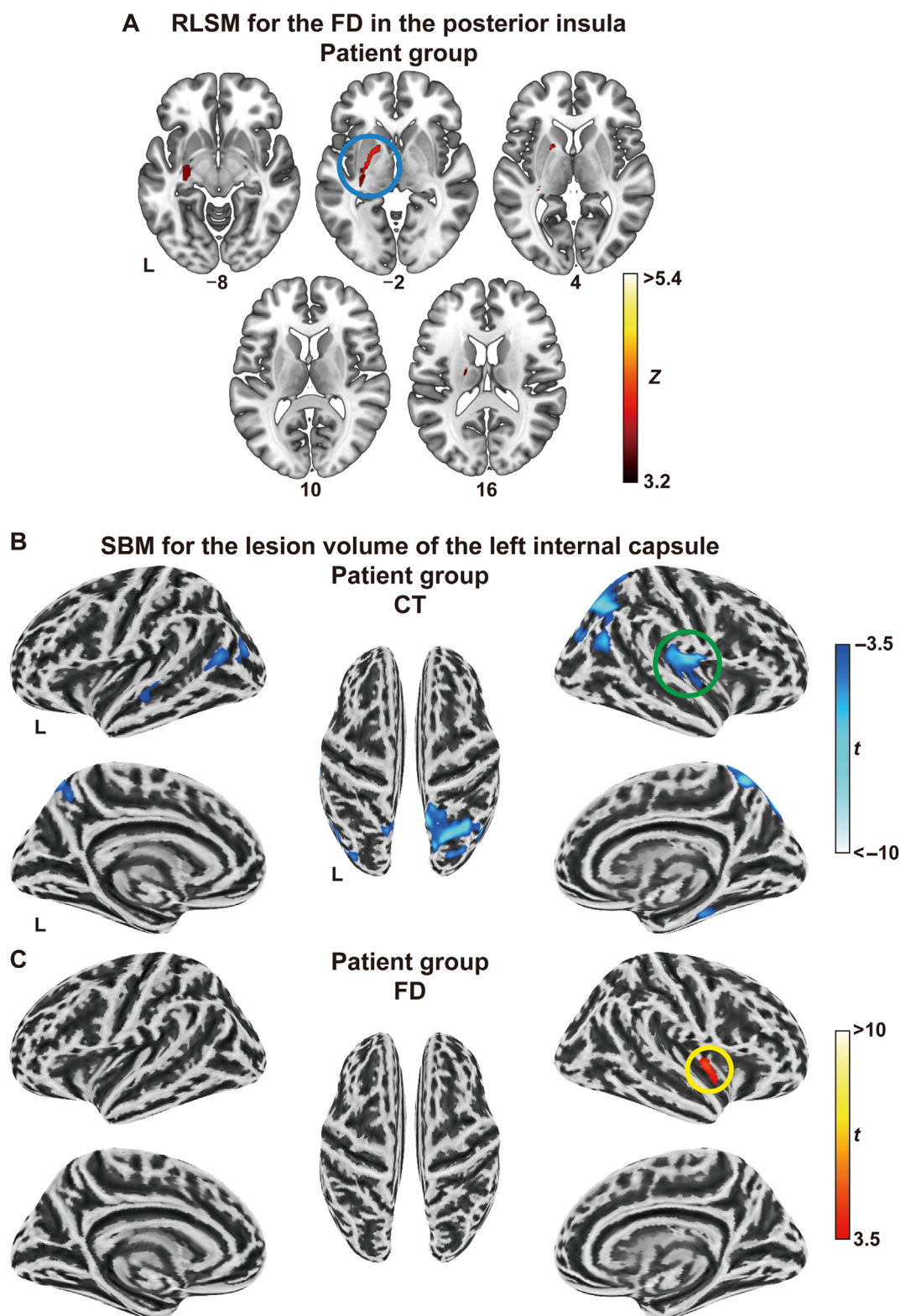


**Fig. 6** – Relationships between a diffuse glioma in the posterior limb of the left internal capsule and cortical structural alterations in the right posterior insula. (A) RLSM for the fractal dimension of the right PI. The color bar denotes the Z-value of each region, which represents the *increased* fractal dimension for the patient group with a diffuse glioma in the ROI. Note the consistency between the results identified by the RLSM for the fractal dimension (blue circle) and the results identified by the RLSM for the factor 1 score (the blue circle in Fig. 3). (B, C) Brain regions with significantly *decreased* cortical thickness (B) and *increased* fractal dimension (C), which were associated with *increased* lesion volumes for the patient group. Note the spatial consistency of the right PI (see Fig. 4) for both cortical thickness (green circles) and fractal dimension (yellow circles).

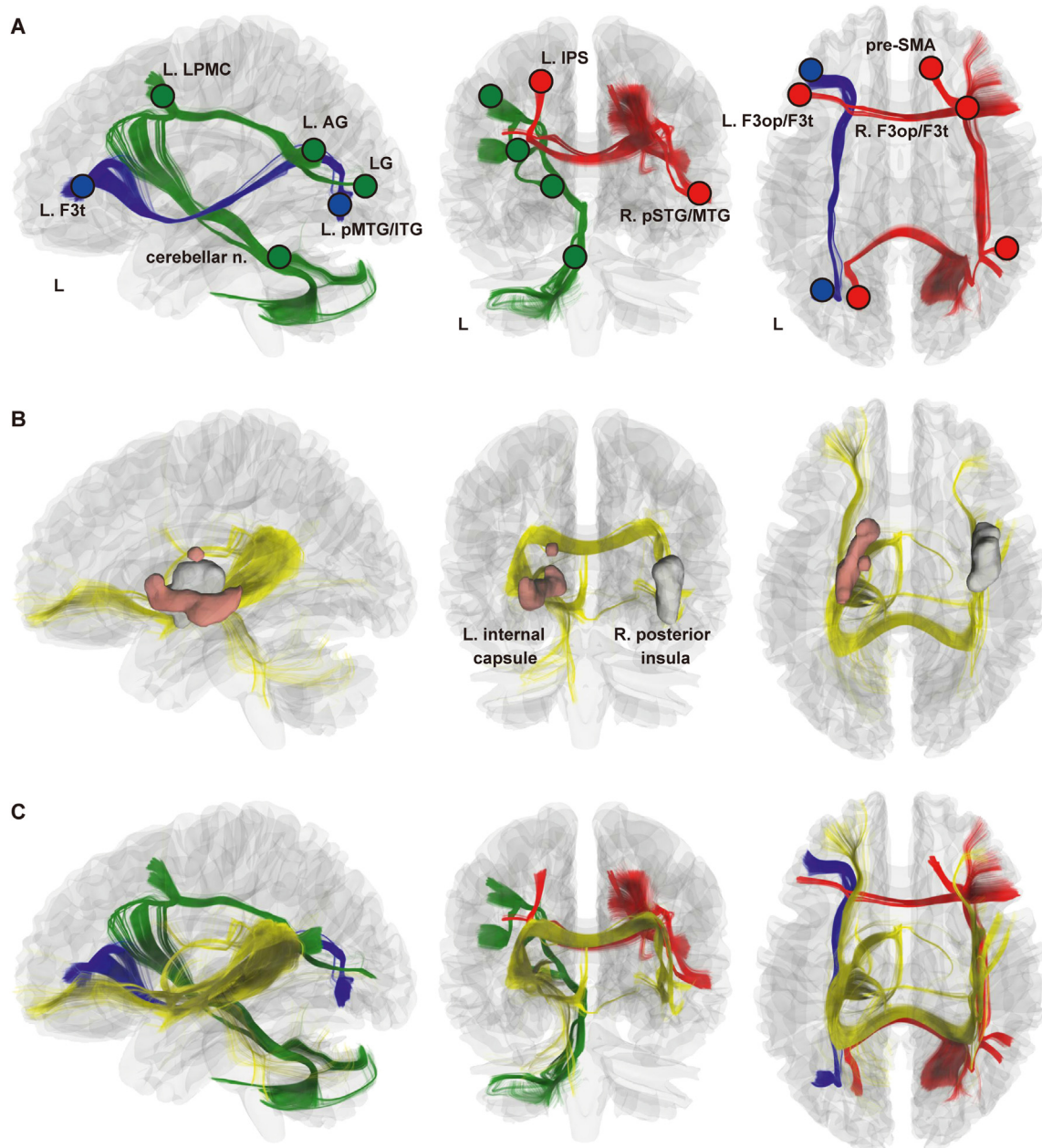


**Fig. 7 – Anatomical connections including the posterior limb of the left internal capsule and right posterior insula. The results of the deterministic fiber tracking using the HCP-842 template (2-mm resolution), which was constructed by MRI diffusion data from 842 subjects (the Human Connectome Project), are shown in the left lateral, posterior, and dorsal views of the standard brain. (A) Anatomical connections for the three syntax-related networks (in red, green, and blue), which were replicated from our previous two-ROI approach using 14 ROIs (Kinno et al., 2014). (B) Anatomical connections identified by the two ROIs of the left PLIC and right PI (in yellow). The left PLIC identified by the RLSM (Fig. 6A) consisted of two separate regions. The ROI of the right PI was determined by the HCP multi-modal parcellation (HCP-MMP) atlas (Glasser et al., 2016). (C) The overlap maps between anatomical connections for the syntax-related networks (A) and those identified by the present study (B), showing their spatial overlaps.**

there were no differences between the groups under the other conditions (all,  $P > .18$ ), including the one-argument and Cont task conditions (both,  $P > .21$ ), suggesting that the general problem-solving abilities, such as word recognition, visual perception, or executive function skill, were controlled between the groups.

A repeated measures MANOVA on the RTs showed significant main effects of group [ $F(1, 49) = 29.17, P < .001$ ] and condition [ $F(3.00, 146.81) = 82.20, P < .001$ ], but without a significant interaction between them [ $F(3.00, 146.81) = 2.66, P = .051$ ]. The patient group showed significantly longer RTs than the control group under all conditions (all,  $P < .001$ ),

**Table 3 – Factor loadings of the error rates of all participants for the two-factor models with promax rotation.**

	Factor 1	Factor 2
Act	<b>.88</b>	–.15
Act+	<b>.79</b>	.13
Pas	<b>.98</b>	–.095
Pas+	<b>.74</b>	.25
Pot	.014	<b>.72</b>
Pot+	–.030	<b>.67</b>
Eigenvalue	3.38	1.73
% of variance	56.33	22.81

Items with a factor loading >.60 (shown in bold) were considered components of the given factor. The number of factors was identified by the Kaiser criterion (eigenvalue >1.00). The inter-factor correlation between Factors 1 and 2 was .33.

including the one-argument and Cont task conditions (both,  $P < .001$ ). No condition-specific effects were observed for the RTs.

The inter-correlation matrix for the error rates of all participants (Table 2) showed a number of significant correlations, which could be divided into multiple factors. The exploratory factor analysis revealed a two-factor structure (Table 3). Factor 1, which had an eigenvalue of 3.38, reflected the error rates of Act, Act+, Pas, and Pas+, and accounted for 56.33% of the variance. The factor 1 scores for the control and patient groups were  $-.16 \pm .11$  and  $.13 \pm .23$  (mean  $\pm$  standard error of the mean), respectively. Factor 2, which had an eigenvalue of 1.73, reflected the error rates of Pot and Pot+, and accounted for 22.31% of the variance. The factor 2 scores for the control and patient groups were  $-.45 \pm .15$  and  $.37 \pm .14$ , respectively. The patient group had significantly higher factor 2 scores than the control group [ $t(49) = 3.9, P < .001$ ], indicating stronger effects for the patients, while there was no significant difference in the factor 1 scores between the groups [ $t(49) = 1.1, P = .29$ ].

### 3.2. Agrammatic comprehension associated with a diffuse glioma in the posterior limb of the left internal capsule

To identify the lesion responsible for the agrammatic comprehension associated with each factor, we performed an RLSM analysis for the factor scores using the JHU neuroanatomical atlas (Fig. 3A). We found that the patients with a diffuse glioma in the left PLIC (“PLIC patients”,  $n = 13$ ) showed a significantly higher score for factor 1 than those with a diffuse glioma in other regions (“other patients”,  $n = 15$ ) (Fig. 3B). No region was significantly associated with factor 2 scores.

To further examine the effects of glioma in the left PLIC on both scores, we compared the factor scores of the PLIC patients or the other patients with those of the control group. Factor 1 scores were  $.61 \pm .47$  for the PLIC patients, and  $-.29 \pm .06$  for the other patients; factor 2 scores were  $.60 \pm .19$  for the PLIC patients, and  $.16 \pm .20$  for the other patients. The factor scores showed no significant correlation with the age of each group

(all,  $P > .11$ ) or the IQ of patients (all,  $P > .51$ ). A repeated measures MANOVA with two factors [group (PLIC patients, other patients, control)  $\times$  factor score (factor 1, factor 2)] showed a significant main effect of group [ $F(2, 48) = 7.73, P = .001$ ], but without a significant main effect of factor score [ $F(1, 48) = .13, P = .72$ ] or their interaction [ $F(2, 48) = 2.59, P = .085$ ]. According to the Dunnett test, only the PLIC patients showed significantly higher factor 1 scores than the control group (PLIC patients:  $P = .037$ ; other patients:  $P = .90$ ), whereas both patient groups showed significantly higher factor 2 scores (PLIC patients:  $P < .001$ ; other patients:  $P = .029$ ). Taken together with the results of the exploratory factor analysis (Table 3), these results indicate that the deficits for the processing of active and passive sentences were associated with a diffuse glioma in the left PLIC, whereas the deficits for the processing of more demanding potential sentences were generally associated with a diffuse glioma in the left hemisphere.

To clarify whether factor 1 was associated with syntactic abilities, we examined the effect of differences in error rates between syntactically more complex and syntactically less complex sentences. Specifically, we focused on the effect of “object scrambling” and performed an RLSM analysis for the differences in error rates between scrambled sentences and subject-initial sentences, i.e.,  $(Act_+ + Pas_+) - (Act + Pas)$ . Our results revealed a significant association between larger differences in the error rates [ $(Act_+ + Pas_+) - (Act + Pas)$ ] and a glioma in the left PLIC (Fig. 3C).

To further examine the effects of a glioma in the left PLIC on the comprehension of scrambled sentences, we compared the differences in the error rates [ $(Act_+ + Pas_+) - (Act + Pas)$ ] between the PLIC patients or other patients and the control group. The differences in error rates [ $(Act_+ + Pas_+) - (Act + Pas)$ ] were  $9.29\% \pm 1.57$  for the PLIC patients,  $3.33\% \pm 1.46$  for the other patients, and  $4.17\% \pm 1.18$  for the control group. The differences in the error rates [ $(Act_+ + Pas_+) - (Act + Pas)$ ] showed no significant correlation with age of each group (all,  $P > .11$ ) or the IQ of patients (both,  $P > .48$ ). An ANOVA with one factor of group showed a significant main effect [ $F(2, 48) = 4.59, P = .015$ ] for the differences in the error rates [ $(Act_+ + Pas_+) - (Act + Pas)$ ]. According to the Dunnett test, only the PLIC patients exhibited a significantly larger difference than the control group (PLIC patients:  $P = .023$ ; other patients:  $P = .88$ ). These results indicate that patients with a diffuse glioma in the left PLIC had deficits in the comprehension of syntactically more complex sentences, suggesting agrammatic comprehension.

### 3.3. Cortical structural variations associated with syntactic abilities

We next performed SBM analysis for the factor scores to determine which cortical structures were associated with syntactic abilities for the healthy participants and patients with a diffuse glioma. We found that the control group had significantly decreased cortical thickness in the right PI and left superior frontal gyrus, both of which were associated with the factor 2 score (Fig. 4A), whereas there was no region associated with the factor 1 score. Regarding the fractal dimension, we found no significant results for either factor 1 or factor 2.

These results demonstrated the individual differences in the structure of the healthy brain that were associated with the comprehension of potential sentences.

On the other hand, the patient group had significantly *decreased* cortical thickness in the right PI, right superior parietal gyrus, and bilateral inferior parietal gyrus, all of which were associated with the factor 1 score (Fig. 4B), whereas there were no regions that were significantly associated with the factor 2 score. Moreover, we found significantly *increased* fractal dimensions in the right PI, precentral gyrus, and cuneus, all of which were associated with the factor 1 score (Fig. 4C). It is interesting to note that the significant region in the right PI for the control group (Fig. 4A) and that for the patient group (Fig. 4B) were partially overlapped (34 vertices).

To clarify whether agrammatic comprehension is affected by cortical structural alterations, we focused on the effects of object scrambling and conducted an SBM analysis for the differences in the error rates  $[(Act_+ + Pas_+) - (Act + Pas)]$ . The results of this analysis revealed a pattern similar to that obtained for factor 1. Indeed, the patient group had significantly *decreased* cortical thickness (Fig. 5A) and *increased* fractal dimension in the right PI (Fig. 5B), which were associated with the *larger* differences in the error rates  $[(Act_+ + Pas_+) - (Act + Pas)]$ . These results suggest that the cortical structural variations in the right PI are associated with the comprehension of syntactically more complex sentences.

### 3.4. Relationships between the glioma location and cortical structural alterations

The neuroimaging results for the behavioral data (Figs. 3–5) demonstrated that agrammatic comprehension was associated not only with a diffuse glioma in the left PLIC, but also with the cortical structural alterations in the right PI. To clarify the relationships between the glioma location and cortical structural alterations, we performed an RLSM analysis in which the cortical parameters (i.e., cortical thickness and fractal dimension) in the right PI were used as variables. We found that the patients with a diffuse glioma in the left PLIC showed significantly *increased* fractal dimensions compared to the other patients (Fig. 6A), whereas there was no region significantly associated with the cortical thickness. Interestingly, there was a spatial overlap between the region identified by the RLSM for the factor score (Fig. 3B) and that for the fractal dimension in the right PI (Fig. 6A).

We next performed an SBM analysis in which the lesion volume of the left PLIC was used as the variable. For this analysis, the overlapped regions between the normalized lesion data of each patient and the resultant image of RLSM (Fig. 3B) were determined as the lesion volume of the left PLIC. The patient group showed significantly *decreased* cortical thickness in the right PI, right superior parietal gyrus, and bilateral inferior parietal gyrus, all of which were associated with an *increased* lesion volume of the left PLIC (Fig. 6B). Moreover, we found a significantly *increased* fractal dimension in the right PI (Fig. 6C). Notably, these regions in the right PI were spatially overlapped with those identified by the SBM for the factor scores (Fig. 4B and C). Collectively, these results indicate that there is a close anatomical link between the left PLIC and right PI.

### 3.5. Anatomical connections between the posterior limb of the left internal capsule and right posterior insula

To confirm the anatomical connections between the left PLIC and right PI, we performed fiber tracking on the human population-averaged diffusion MRI template. First, we confirmed all of the anatomical connections among the 14 critical regions identified previously (Fig. 7A) (Kinno et al., 2014), which could be functionally classified into three syntax-related networks: Network I (the opercular/triangular parts of the left inferior frontal gyrus, left intraparietal sulcus, right frontal regions, presupplementary motor area, and right temporal regions), Network II (the left lateral premotor cortex, left angular gyrus, lingual gyrus, and cerebellar nuclei), and Network III (the left ventral frontal and posterior temporal regions).

Next, we tracked the fibers that passed through both the left PLIC and the right PI (Fig. 7B). In both hemispheres, the fibers mainly consisted of the extreme capsule (EmC), middle longitudinal fasciculus (MdLF), and inferior longitudinal fasciculus (ILF), and they reached the inferior frontal gyrus. The left PLIC and right PI were anatomically connected via the splenium of the corpus callosum, and these fibers reached the left cerebellum via the left thalamus. Moreover, we found that these fibers were actually a part of the three syntax-related networks (Fig. 7C): the fibers passing through the splenium of the corpus callosum and the right EmC, right MdLF, and right ILF overlapped with Network I, the fibers reaching the left cerebellum via the left thalamus overlapped with Network II, and the fibers passing through the left EmC, left MdLF, and left ILF overlapped with Network III. These results demonstrate that the route between the left PLIC and the right PI is anatomically integrated into the syntax-related networks.

## 4. Discussion

Our combined analysis of the behavioral and neuroimaging data demonstrates the importance of the left PLIC and the right PI for preserving syntactic abilities in patients with a diffuse glioma. The RLSM revealed clear associations between agrammatic comprehension and a diffuse glioma in the left PLIC (Fig. 3), whereas the SBM showed that *decreased* cortical thickness and/or *increased* complexity of the right PI were associated not only with agrammatic comprehension of the patients but also with the syntactic abilities of healthy participants (Figs. 4 and 5). Moreover, there was a close anatomical link between these two regions, such that the *higher* glioma volume in the left PLIC was associated with the *decreased* cortical thickness and *increased* fractal dimension in the right PI (Fig. 6). Furthermore, the route between these two regions was anatomically integrated into the preexisting syntax-related networks (Fig. 7) (Kinno et al., 2014). These results indicate that syntactic abilities in the patients with a diffuse glioma were closely related to the structural variations not only of the particular tract but also of the cortical region, both of which are closely associated with the syntax-related networks.

The specific deficits in the comprehension of scrambled sentences observed in patients with a diffuse glioma in the left PLIC (Fig. 3C) indicate agrammatic comprehension. Patients

with agrammatic comprehension tend to have difficulty comprehending sentences with noncanonical structure (Caramazza & Zurif, 1976; Kinno et al., 2009, 2014; Thompson & Choy, 2009), which supports our interpretations. The internal capsule is composed of a continuous sheet of white matter fibers that travel through the basal ganglia and connect the cortex, brainstem, and spinal cord, as well as the basal ganglia and thalamus (Cowan & de Vries, 2005). Damage to the internal capsule causes a disconnection between these regions, resulting in severe motor or sensory loss. The alterations of the functional connectivity between the left frontal regions and other regions within the syntax-related networks in agrammatic patients (Kinno et al., 2014, 2015) can be explained by a disconnection due to a diffuse glioma in the left PLIC. That this functional connectivity is important for syntactic abilities is further supported by the results of a VLSM study of stroke patients with agrammatic comprehension (den Ouden et al., 2019). Therefore, it is natural to assume that a diffuse glioma in the left PLIC (Fig. 3B and C) affects this functional connectivity. Damage to the internal capsule and left frontal regions has been observed in patients with the non-fluent/agrammatic variant of primary progressive aphasia (naPPA), whose clinical features include syntactic deficits for the comprehension of complex sentences (Gorno-Tempini et al., 2011; Grossman, 2012; Kinno et al., 2017; Mandelli et al., 2016). Taken together, these results indicate that a diffuse glioma in the left PLIC would lead to a disconnection between the frontal regions and other regions within the identified syntax-related networks, which would be one reason for agrammatic comprehension.

The cortical structural variations of the right PI were found to be associated with the behavioral data of both patients and healthy controls (Figs. 4 and 5). In the brains of patients, these variations were associated not only with factor 1 but also with the comprehension of syntactically more complex sentences, indicating a potential association between these variations and the syntactic abilities of patients. Conversely, in the healthy brains, these variations were associated with the comprehension of the potential sentences (Fig. 4A). One plausible explanation is that the variations were linked to syntactic abilities in the healthy brain; this is supported by the overlap between the significant regions in the right PI of the control group (Fig. 4A) and the patient group (Fig. 4B). A meta-analysis of neuroimaging studies has demonstrated the functional role of the right insula in the comprehension of scrambled sentences (Walenski, Europa, Caplan, & Thompson, 2019). In addition, enhanced activation in the right insula during the processing of the scrambled active sentences has been reported (Kinno et al., 2008). Another possibility is that the right PI plays diverse functional roles in supporting the comprehension of syntactically more complex sentences. The insula is known as a major multimodal network hub in the cerebral cortex, playing major roles in language, sensation, auditory, visual, limbic, and vestibular functions, as well as saliency processing (Dionisio et al., 2019). Previous studies have reported the difficulty of comprehending potential sentences for healthy participants (Tamaoka et al., 2005; Tanaka et al., 2017). This difficulty may arise from entrenched beliefs regarding case markers—e.g., that a case marker *-ga* always represents the subject in a task,

although a noun with a case marker *-ga* is the subject in active and passive sentences, whereas a noun with a case marker *-ni* is the subject in potential sentences (Ura, 1999). It is important to control such entrenched beliefs in order to accurately comprehend potential sentences, and the right PI may contribute to this process. Additionally, considering that patients with diffuse gliomas in the left hemisphere exhibit impaired attention and working memory (Habets et al., 2019), and that all patients in our study had greater difficulty in understanding potential sentences compared to healthy controls (Fig. 2), these functions may be related to the right PI. Given the diverse functional roles of the insula, we concluded that the contribution of the right PI varies depending on syntactic load, such that the right PI plays a crucial role in supporting syntactic abilities in cases where syntactic abilities are disturbed, or it serves various supportive roles in processing more complex sentences.

The cortical thickness and fractal dimension in the right PI exhibited inverse variation, such that syntactic abilities were negatively associated with decreased cortical thickness and increased fractal dimension (Figs. 4 and 5). These findings are consistent with previous studies that reported similar patterns of structural alterations, such as increased cortical thickness with decreased fractal dimension (Im et al., 2006; Jiang et al., 2008). It is worth noting that computer simulations of cortical folding have also demonstrated that thicker cortical layers exhibit less convolution (Toro & Burnod, 2005), which is consistent with the present findings. Importantly, the observed cortical structural alterations were not limited to patients; they were also observed in healthy controls, suggesting that these changes cannot be attributed solely to the presence of tumor. Here, the increased cortical thickness can be explained by structural plasticity, which is triggered by various factors including experience, training, environment, stress, and injury, and can impact human behaviour (Kolb & Whishaw, 1998). Notably, a glioma invades eloquent brain areas, triggering disinhibition of nearby neural networks (Pasquini, Di Napoli, et al., 2022). Structural plasticity can induce changes in synapses, axons, and myelin coating, resulting in cortical thickening. Such cortical thickening may stem from multiple factors, including larger cell size, higher spine density, the generation of new neural or glial cells, or slower-developing processes such as changes in myelin plasticity, axonal sprouting, or angiogenesis (Almairac et al., 2018). Taken together, these findings suggest that individual differences in the structure of the right PI reflect variable contributions to the comprehension of syntactically more complex sentences.

There were spatial overlaps between the regions identified for the behavioral data (Figs. 4 and 5) and those identified for the structural parameters such as the glioma volume of the left PLIC or cortical fractal dimension of the right PI (Fig. 6). The anatomical link between the glioma volume in the left PLIC and the cortical structural variations in the right PI would thus be associated with the syntactic abilities. This anatomical link appears to be related to the structural reorganization compensating for the damage to syntax-related networks; that is, the increased cortical thickness in the right PI contributes to the preserved syntactic abilities of patients with glioma. Previous voxel-based morphometry (VBM) studies have

reported increased gray matter volume in the right insula in patients with a glioma in the left insula (Almairac et al., 2018; Pasquini, Jenabi, Peck, & Holodny, 2022). As the syntax-related networks extend throughout the whole brain (Fig. 7), gliomas in the left hemisphere partially affect this network in all patients. Nevertheless, the absence of agrammatic comprehension may be partly attributed to structural reorganization (i.e., a thicker cortical thickness) in the right PI. On the other hand, the structural reorganization is disturbed in patients with a glioma in the left PLIC. A possible mechanism for this disturbance is that the disconnection by the glioma in the left PLIC prevents the utilization of incompletely damaged syntax-related networks, which are essential for successful neuroplasticity (Berthier et al., 2011), and such insufficient reorganization results in agrammatic comprehension.

There are several fibers connecting the left PLIC and the right PI (Fig. 7). In our patients the left ventral pathway was found to be composed of several fibers in which each of the EmC, MdLF, and ILF were partially involved. These fibers have been associated with the ventral stream in the dual stream model for speech processing (Hickok & Poeppel, 2007). Although the concept of the dual stream model is generally accepted, its anatomical details remain controversial (Dick & Tremblay, 2012). A recent post-mortem investigation has demonstrated that the left PLIC joins the sagittal striatum to the posterior part of the left MdLF (Aydin & Aydin, 2020). Regarding their functional roles, the left ventral pathway would be included in the syntax-related networks for the interactions between syntax and semantics (Kinno et al., 2014). A glioma in the left PLIC would be expected to affect this connection, resulting in deficits of those interactions.

We also found fibers reaching the left cerebellum via the left thalamus, and these were also included in the syntax-related networks (Fig. 7). These fibers are considered to be part of the cerebello-thalamo-cortical pathways connecting the cerebral cortex (particularly the prefrontal cortex) and cerebellum (Ramnani, 2006). The lateral ventral nuclei of the thalamus is the major relay for these pathways (Morel, Magnin, & Jeanmonod, 1997). The internal capsule conveys information from the primary and supplementary motor areas, frontopontine, and thalamic peduncles to the brain stem and cerebellar regions, as well as from the thalamus to the prefrontal cortex (Sullivan, Zahr, Rohlfing, & Pfefferbaum, 2010). This pathway plays a functional role not only in motor function but also in cognitive processing (Bodranghien et al., 2016). Previous studies have demonstrated a relationship between cerebellar lesions and syntactic deficits (Adamaszek, Strecker, & Kessler, 2012; Cook, Murdoch, Cahill, & Whelan, 2004). Among the syntax-related networks, this pathway is crucial for syntactic processing and the input/output interface (Kinno et al., 2014). The present findings further suggest that damage to this pathway would affect syntactic abilities.

The present study has focused on the right ventral pathway, including the right EmC, right MdLF, and right ILF (Fig. 7B). The right ventral pathway connects the right PI and other syntax-related regions; this pathway was not included in the syntax-related networks previously identified (Fig. 7A). A previous fMRI study showed that the right EmC and right PI are associated with more demanding syntactic processing, such as thematic role assignment (Frankland & Greene, 2015).

We also showed that the cortical structural alterations in the right PI were associated with the processing of potential sentences (Fig. 4A), which was more demanding syntactic processing even for the healthy participants (Fig. 2C). Moreover, the functional role of the right ventral pathway is also assumed to be a supporting role for the left homologous pathway. According to a previous study, activations during auditory sentence processing showed strong interhemispheric interactions via the corpus callosum (Saur et al., 2010). Given that the cortical structural alterations in the right PI and the right ventral pathway were identified on MR images of the healthy participants (Figs. 4 and 7), we concluded that the right ventral pathway belongs to the syntax-related networks, and that its function depends on syntactic loads.

The observation that right hemisphere homologs contribute to language recovery in patients with left hemisphere lesions supports the hypothesis of a bilateral parallel language network (Crinion & Price, 2005; Saur et al., 2006). A recent fiber tracking study examined the contribution of the right tracts to the linguistic abilities of aphasic patients, and found negative correlations between the linguistic abilities of the patients and radial diffusivity in the right EmC (Kourtidou et al., 2021). Because lower radial diffusivity has been linked to decreased axonal demyelination (Alexander, Lee, Lazar, & Field, 2007), this finding indicates the importance of the right tracts for the recovery after aphasia. Our present findings further suggest that the variable contribution of the right ventral pathway to syntactic abilities depends on individual deficits, and that the recovery from agrammatic comprehension would be closely associated with the syntax-related networks. We can safely assume that functional recovery in language would be primarily achieved by changing the manner of neural connections among critical regions, rather than by creating new neural connections outside the pre-existing networks.

Although we used standard protocols for data analysis, it is necessary to discuss several potential limitations in regard to the analysis of neuroimaging data in this study. First, the glioma location based on the normalized images may differ slightly from the actual location of the glioma. To minimize these differences, we applied the same registration algorithm as in previous VBM studies (Almairac et al., 2018; Yuan et al., 2020; Zhang et al., 2018), which has been shown to be acceptable for spatial normalization of the lesioned brain (Ripollés et al., 2012). In addition, all resultant images were visually verified to be free of artifacts and deformations, and passed the quality and homogeneity checking algorithms implemented in the CAT12 Toolbox. Therefore, the left PLIC was almost certainly included in the responsible regions for agrammatic comprehension. However, considering the limitations of image processing, it is possible that the responsible regions included not only the left PLIC but the adjacent left insula. Secondly, more overlapped regions could have been observed, if the vertex-level threshold or FWHM for the smoothing were relieved in the SBM analysis. However, the use of lower thresholds increases the high risk of false positive results (Greve & Fischl, 2018). Nevertheless, we were able to identify overlapped regions in the right PI with a conservative threshold. Thirdly, the fiber tracking techniques cannot separate microstructures that are smaller than the image

resolution (Campbell & Pike, 2014). It is likely that a voxel in a single fiber pathway included a mixture of other fiber pathways, gray matter, and cerebrospinal fluid; the percentage of voxels with multiple fiber tracts is estimated to be as high as 90% (Jones, 2010). Moreover, even a voxel in a straight pathway may include curved or splayed fibers. Therefore, the anatomical connections between the left PLIC and the right PI may not be direct pathways. Considering these limitations of the current neuroimaging techniques, further fine-scale histological studies with the post-mortem human brain are required to validate the present findings. Finally, the effect of age on cortical structural alterations should be considered. A previous study suggested that younger individuals (18–31 years) have significantly greater cortical thickness than their middle-aged counterparts (41–57 years) (Salat et al., 2004). While there were no significant differences in age among the groups in our study, it is important to acknowledge that the effects of age differences on cortical structural alterations cannot be completely ruled out. To address this issue, age was included as a nuisance factor in the SBM analyses. Moreover, neither the factor scores nor the differences in the error rates [(Act<sub>+</sub> + Pas<sub>+</sub>) – (Act + Pas)] showed any correlation with age. These procedures would minimize the effects of age differences on cortical structural alterations.

## 5. Conclusions

We successfully demonstrated that the syntactic abilities in patients with a diffuse glioma were closely associated with cortical structural alterations of the syntax-related networks. It has been reported that surgical excision of the eloquent areas, including the left inferior frontal gyrus, may not necessarily result in severe post-operative aphasia, as determined by clinical follow-up visits (Desmurget et al., 2007). In a prior study on patients with diffuse glioma, only 15% of patients failed to fully recover, and these individuals only demonstrated syntactic processing abnormalities for the more complex syntactic structures (Teichmann et al., 2015). Syntactic abilities may be preserved after tumor removal in an eloquent area due to post-operative reorganization that is closely associated with the syntax-related networks (Kinno, Chang, & Friederici, 2021). During the postoperative period, the other regions may make a greater contribution to the syntactic processing. The bilateral networks between the left PLIC and the right PI (Fig. 7) may be a critical feature in the post-operative reorganization of these networks. This could help explain why some patients experience acute post-operative syntactic deficits after the eloquent area is removed, while others recover over time. Further data on post-hoc reorganization is required in order to fully elucidate the syntactic abilities of patients with diffuse gliomas or strokes.

## Data availability

The data supporting the findings of this study are not publicly available due to information that could compromise the privacy of the research participants but are available from the

corresponding author (RK) upon request and after meeting the conditions established by the local ethical committee (i.e., the conditions of the data sharing agreement). Legal copyright restrictions prevent the public archiving of the experimental materials, including the presentation code and analysis code used in this experiment. These materials can be obtained from the copyright holders in the cited references (see 2. Materials and methods). No part of the study procedures or analysis plans was preregistered prior to the research being conducted. We report how we determined our sample size, all data exclusions, all inclusion/exclusion criteria, whether inclusion/exclusion criteria were established prior to data analysis, all manipulations, and all measures in the study.

## CRediT author contributions

**Ryuta Kinno:** Conceptualization; Data curation; Formal analysis; Funding acquisition; Investigation; Methodology; Project administration; Resources; Software; Visualization; Writing – original draft preparation; Writing – review & editing. **Yoshihiro Muragaki:** Resources; Supervision; Writing – review & editing. **Takashi Maruyama:** Resources. **Manabu Tamura:** Investigation; Project administration; Resources. **Kenjiro Ono:** Funding acquisition; Supervision. **Kyohei Tanaka:** Investigation; Methodology; Visualization. **Kuniyoshi L. Sakai:** Conceptualization; Supervision; Visualization; Writing – original draft preparation; Writing – review & editing.

## Declaration of competing interest

The authors declare that they have no known competing financial interests or personal relationships that could have appeared to influence the work reported in this paper.

## Acknowledgements

We thank N. Komoro for technical assistance, and H. Matsuda and H. Kawano for administrative assistance. This work was supported by a Grant-in-Aid for Scientific Research (C) (#JP 23K00487) from the Japan Society for the Promotion of Science, and a grant from the Brain Science Foundation.

## REFERENCES

- Adamaszek, M., Strecker, K., & Kessler, C. (2012). Impact of cerebellar lesion on syntactic processing evidenced by event-related potentials. *Neuroscience Letters*, 512(2), 78–82. <https://doi.org/10.1016/j.neulet.2012.01.020>
- Alexander, A. L., Lee, J. E., Lazar, M., & Field, A. S. (2007). Diffusion tensor imaging of the brain. *Neurotherapeutics: the Journal of the American Society for Experimental Neurotherapeutics*, 4(3), 316–329. <https://doi.org/10.1016/j.nurt.2007.05.011>
- Almairac, F., Duffau, H., & Herbert, G. (2018). Contralesional macrostructural plasticity of the insular cortex in patients with glioma: A VBM study. *Neurology*, 91(20), e1902–e1908. <https://doi.org/10.1212/WNL.0000000000006517>

- Ashburner, J. (2007). A fast diffeomorphic image registration algorithm. *Neuroimage*, 38(1), 95–113. <https://doi.org/10.1016/j.neuroimage.2007.07.007>
- Aydin, S., & Aydin, A. (2020). Microsurgical anatomy of middle longitudinal fasciculus. *Annals of Medical Research*, 27(10), 2683. <https://doi.org/10.5455/annalsmedres.2020.05.426>
- Bartlett, M. S. (1950). Tests of significance in factor analysis. *The British Journal of Social Psychology*, 3(2), 77–85.
- Bartolomei, F., Bosma, I., Klein, M., Baayen, J. C., Reijneveld, J. C., Postma, T. J., ... de Jongh, A. (2006). How do brain tumors alter functional connectivity? A magnetoencephalography study. *Annals of Neurology*, 59(1), 128–138.
- Berthier, M. L., Garcia-Casares, N., Walsh, S. F., Nabrozidis, A., Ruiz de Mier, R. J., Green, C., ... Pulvermuller, F. (2011). Recovery from post-stroke aphasia: Lessons from brain imaging and implications for rehabilitation and biological treatments. *Discovery Medicine*, 12(65), 275–289.
- Bodranghien, F., Bastian, A., Casali, C., Hallett, M., Louis, E. D., Manto, M., ... van Dun, K. (2016). Consensus paper: Revisiting the symptoms and signs of cerebellar syndrome. *The Cerebellum*, 15(3), 369–391. <https://doi.org/10.1007/s12311-015-0687-3>
- Campbell, J. S., & Pike, G. B. (2014). Potential and limitations of diffusion MRI tractography for the study of language. *Brain and Language*, 131, 65–73. <https://doi.org/10.1016/j.bandl.2013.06.007>
- Caramazza, A., & Miceli, G. (1991). Selective impairment of thematic role assignment in sentence processing. *Brain and Language*, 41(3), 402–436. [https://doi.org/10.1016/0093-934x\(91\)90164-v](https://doi.org/10.1016/0093-934x(91)90164-v)
- Caramazza, A., & Zurif, E. B. (1976). Dissociation of algorithmic and heuristic processes in language comprehension: Evidence from aphasia. *Brain and Language*, 3(4), 572–582. [https://doi.org/10.1016/0093-934x\(76\)90048-1](https://doi.org/10.1016/0093-934x(76)90048-1)
- Cook, M., Murdoch, B., Cahill, L., & Whelan, B. M. (2004). Higher-level language deficits resulting from left primary cerebellar lesions. *Aphasiology*, 18(9), 771–784.
- Cowan, F. M., & de Vries, L. S. (2005). The internal capsule in neonatal imaging. *Seminars in Fetal & Neonatal Medicine*, 10(5), 461–474. <https://doi.org/10.1016/j.siny.2005.05.007>
- Crinion, J., & Price, C. J. (2005). Right anterior superior temporal activation predicts auditory sentence comprehension following aphasic stroke. *Brain: a Journal of Neurology*, 128(Pt 12), 2858–2871. <https://doi.org/10.1093/brain/awh659>
- Dahnke, R., Yotter, R. A., & Gaser, C. (2013). Cortical thickness and central surface estimation. *Neuroimage*, 65, 336–348. <https://doi.org/10.1016/j.neuroimage.2012.09.050>
- de Groot, M., Reijneveld, J. C., Aronica, E., & Heimans, J. J. (2012). Epilepsy in patients with a brain tumour: Focal epilepsy requires focused treatment. *Brain: a Journal of Neurology*, 135(Pt 4), 1002–1016. <https://doi.org/10.1093/brain/awr310>
- de Winter, J. C., Dodou, D., & Wieringa, P. A. (2009). Exploratory factor analysis with small sample sizes. *Multivariate Behavioral Research*, 44(2), 147–181. <https://doi.org/10.1080/00273170902794206>
- den Ouden, D. B., Maljutina, S., Basilakos, A., Bonilha, L., Gleichgerrcht, E., Yourganov, G., ... Fridriksson, J. (2019). Cortical and structural-connectivity damage correlated with impaired syntactic processing in aphasia. *Human Brain Mapping*, 40(7), 2153–2173.
- Desmurget, M., Bonnetblanc, F., & Duffau, H. (2007). Contrasting acute and slow-growing lesions: A new door to brain plasticity. *Brain: a Journal of Neurology*, 130(Pt 4), 898–914. <https://doi.org/10.1093/brain/awl300>
- Dick, A. S., & Tremblay, P. (2012). Beyond the arcuate fasciculus: Consensus and controversy in the connective anatomy of language. *Brain: a Journal of Neurology*, 135(Pt 12), 3529–3550. <https://doi.org/10.1093/brain/aws222>
- Dionisio, S., Mayoglou, L., Cho, S. M., Prime, D., Flanigan, P. M., Lega, B., ... Nair, D. (2019). Connectivity of the human insula: A cortico-cortical evoked potential (CCEP) study. *Cortex; a Journal Devoted To the Study of the Nervous System and Behavior*, 120, 419–442. <https://doi.org/10.1016/j.cortex.2019.05.019>
- Duffau, H. (2005). Lessons from brain mapping in surgery for low-grade glioma: Insights into associations between tumour and brain plasticity. *Lancet Neurology*, 4(8), 476–486.
- Faria, A. V., Joel, S. E., Zhang, Y., Oishi, K., van Zijl, P. C., Miller, M. I., ... Mori, S. (2012). Atlas-based analysis of resting-state functional connectivity: Evaluation for reproducibility and multi-modal anatomy-function correlation studies. *Neuroimage*, 61(3), 613–621. <https://doi.org/10.1016/j.neuroimage.2012.03.078>
- Frankland, S. M., & Greene, J. D. (2015). An architecture for encoding sentence meaning in left mid-superior temporal cortex. *Proceedings of National Academy of Sciences in United States of America*, 112(37), 11732–11737. <https://doi.org/10.1073/pnas.1421236112>
- Friston, K., Ashburner, J., Frith, C. D., Poline, J. B., Heather, J. D., & Frackowiak, R. S. (1995). Spatial registration and normalization of images. *Human Brain Mapping*, 3(3), 165–189.
- Glasser, M. F., Coalson, T. S., Robinson, E. C., Hacker, C. D., Harwell, J., Yacoub, E., ... Van Essen, D. C. (2016). A multi-modal parcellation of human cerebral cortex. *Nature*, 536(7615), 171–178. <https://doi.org/10.1038/nature18933>
- Gorno-Tempini, M. L., Hillis, A. E., Weintraub, S., Kertesz, A., Mendez, M., Cappa, S. F., ... Grossman, M. (2011). Classification of primary progressive aphasia and its variants. *Neurology*, 76(11), 1006–1014. <https://doi.org/10.1212/WNL.0b013e31821103e6>
- Greve, D. N., & Fischl, B. (2018). False positive rates in surface-based anatomical analysis. *Neuroimage*, 171, 6–14. <https://doi.org/10.1016/j.neuroimage.2017.12.072>
- Grossman, M. (2012). The non-fluent/agrammatic variant of primary progressive aphasia. *Lancet Neurology*, 11(6), 545–555.
- Habets, E. J., Hendriks, E. J., Taphoorn, M. J., Douw, L., Zwinderman, A. H., Vandertop, W. P., ... Klein, M. (2019). Association between tumor location and neurocognitive functioning using tumor localization maps. *Journal of Neuro-Oncology*, 144(3), 573–582.
- Hickok, G., & Poeppel, D. (2007). The cortical organization of speech processing. *Nature Reviews. Neuroscience*, 8(5), 393–402. <https://doi.org/10.1038/nrn2113>
- Howard, M. C. (2016). A review of exploratory factor analysis decisions and overview of current practices: What we are doing and how can we improve? *International Journal of Human-Computer Interaction*, 32(1), 51–62.
- Imamura, S., Sato, Y., & Koizumi, M. (2016). The processing cost of scrambling and topicalization in Japanese. *Frontiers in Psychology*, 7, 531. <https://doi.org/10.3389/fpsyg.2016.00531>
- Im, K., Lee, J. M., Yoon, U., Shin, Y. W., Hong, S. B., Kim, I. Y., ... Kim, S. I. (2006). Fractal dimension in human cortical surface: Multiple regression analysis with cortical thickness, sulcal depth, and folding area. *Human Brain Mapping*, 27(12), 994–1003. <https://doi.org/10.1002/hbm.20238>
- Jiang, J., Zhu, W., Shi, F., Zhang, Y., Lin, L., & Jiang, T. (2008). A robust and accurate algorithm for estimating the complexity of the cortical surface. *Journal of Neuroscience Methods*, 172(1), 122–130. <https://doi.org/10.1016/j.jneumeth.2008.04.018>
- Jones, D. K. (2010). Challenges and limitations of quantifying brain connectivity in vivo with diffusion MRI. *Imaging in Medicine*, 2(3), 341–355. <https://doi.org/10.2217/iim.10.21>
- Kaiser, H. F., & Rice, J. (1974). Little jiffy, mark IV. *Educational and Psychological Measurement*, 34(1), 111–117. <https://doi.org/10.1177/001316447403400115>
- Kinno, R., Chang, E., & Friederici, A. D. (2021). Syntax. In E. Mandonnet, & G. Herbet (Eds.), *Intraoperative mapping of cognitive networks* (pp. 155–170). Springer.

- Kinno, R., Kawamura, M., Shioda, S., & Sakai, K. L. (2008). Neural correlates of noncanonical syntactic processing revealed by a picture-sentence matching task. *Human Brain Mapping*, 29(9), 1015–1027.
- Kinno, R., Kii, Y., Kurokawa, S., Owan, Y., Kasai, H., & Ono, K. (2017). Effects of word order and morphological information on Japanese sentence comprehension in nonfluent/agrammatic variant of primary progressive aphasia. *Journal of Neurolinguistics*, 44, 107–119.
- Kinno, R., Muragaki, Y., Hori, T., Maruyama, T., Kawamura, M., & Sakai, K. L. (2009). Agrammatic comprehension caused by a glioma in the left frontal cortex. *Brain and Language*, 110(2), 71–80. <https://doi.org/10.1016/j.bandl.2009.05.001>
- Kinno, R., Muragaki, Y., Maruyama, T., Tamura, M., Tanaka, K., Ono, K., et al. (2020). Differential effects of a left frontal glioma on the cortical thickness and complexity of both hemispheres. *Cerebral Cortex Communications*, 1(1), tga027.
- Kinno, R., Ohta, S., Muragaki, Y., Maruyama, T., & Sakai, K. L. (2014). Differential reorganization of three syntax-related networks induced by a left frontal glioma. *Brain: a Journal of Neurology*, 137(Pt 4), 1193–1212. <https://doi.org/10.1093/brain/awu013>
- Kinno, R., Ohta, S., Muragaki, Y., Maruyama, T., & Sakai, K. L. (2015). Left frontal glioma induces functional connectivity changes in syntax-related networks. *SpringerPlus*, 4(1), 317. <https://doi.org/10.1186/s40064-015-1104-6>
- Kolb, B., & Whishaw, I. Q. (1998). Brain plasticity and behavior. *Annual Review of Psychology*, 49(1), 43–64. <https://doi.org/10.1146/annurev.psych.49.1.43>
- Kourtidou, E., Kasselimis, D., Angelopoulou, G., Karavasilis, E., Velonakis, G., Kelekis, N., ... Petrides, M. (2021). The role of the right hemisphere white matter tracts in chronic aphasic patients after damage of the language tracts in the left hemisphere. *Frontiers in Human Neuroscience*, 15, 635750. <https://doi.org/10.3389/fnhum.2021.635750>
- Louis, D. N., Ohgaki, H., Wiestler, O. D., Cavenee, W. K., Burger, P. C., Jouvett, A., ... Kleihues, P. (2007). The 2007 WHO classification of tumours of the central nervous system. *Acta Neuropathologica*, 114(2), 97–109. <https://doi.org/10.1007/s00401-007-0243-4>
- Luders, E., Narr, K. L., Thompson, P. M., Rex, D. E., Woods, R. P., Deluca, H., ... Toga, A. W. (2006). Gender effects on cortical thickness and the influence of scaling. *Human Brain Mapping*, 27(4), 314–324. <https://doi.org/10.1002/hbm.20187>
- Mandelli, M. L., Vitali, P., Santos, M., Henry, M., Gola, K., Rosenberg, L., ... Gorno-Tempini, M. L. (2016). Two insular regions are differentially involved in behavioral variant FTD and nonfluent/agrammatic variant PPA. *Cortex; a Journal Devoted To the Study of the Nervous System and Behavior*, 74, 149–157. <https://doi.org/10.1016/j.cortex.2015.10.012>
- Morel, A., Magnin, M., & Jeanmonod, D. (1997). Multiarchitectonic and stereotactic atlas of the human thalamus. *Journal of Computational Neurology*, 387(4), 588–630. [https://doi.org/10.1002/\(sici\)1096-9861\(19971103\)387:4<588::aid-cne8>3.0.co;2-z](https://doi.org/10.1002/(sici)1096-9861(19971103)387:4<588::aid-cne8>3.0.co;2-z)
- Motomura, K., Chalise, L., Ohka, F., Aoki, K., Tanahashi, K., Hirano, M., ... Natsume, A. (2019). Neurocognitive and functional outcomes in patients with diffuse frontal lower-grade gliomas undergoing intraoperative awake brain mapping. *Journal of Neurosurgery*, 132(6), 1683–1691. <https://doi.org/10.3171/2019.3.JNS19211>
- Nenadic, I., Yotter, R. A., Sauer, H., & Gaser, C. (2014). Cortical surface complexity in frontal and temporal areas varies across subgroups of schizophrenia. *Human Brain Mapping*, 35(4), 1691–1699. <https://doi.org/10.1002/hbm.22283>
- Ohta, S., Koizumi, M., & Sakai, K. L. (2017). Dissociating effects of scrambling and topicalization within the left frontal and temporal language areas: An fMRI study in Kaqchikel Maya. *Frontiers in Psychology*, 8, 748.
- Oldfield, R. C. (1971). The assessment and analysis of handedness: The Edinburgh inventory. *Neuropsychologia*, 9(1), 97–113. [https://doi.org/10.1016/0028-3932\(71\)90067-4](https://doi.org/10.1016/0028-3932(71)90067-4)
- Pasquini, L., Di Napoli, A., Rossi-Espagnet, M. C., Visconti, E., Napolitano, A., Romano, A., ... Holodny, A. I. (2022a). Understanding Language reorganization with neuroimaging: How language adapts to different focal lesions and insights into clinical applications. *Frontiers in Human Neuroscience*, 16.
- Pasquini, L., Jenabi, M., Peck, K. K., & Holodny, A. I. (2022b). Language reorganization in patients with left-hemispheric gliomas is associated with increased cortical volume in language-related areas and in the default mode network. *Cortex; a Journal Devoted To the Study of the Nervous System and Behavior*, 157, 245–255.
- Ramnani, N. (2006). The primate cortico-cerebellar system: Anatomy and function. *Nature Reviews. Neuroscience*, 7(7), 511–522. <https://doi.org/10.1038/nrn1953>
- Ripollés, P., Marco-Pallarés, J., de Diego-Balaguer, R., Miro, J., Falip, M., Juncadella, M., et al. (2012). Analysis of automated methods for spatial normalization of lesioned brains. *Neuroimage*, 60(2), 1296–1306.
- Salat, D. H., Buckner, R. L., Snyder, A. Z., Greve, D. N., Desikan, R. S., Busa, E., ... Fischl, B. (2004). Thinning of the cerebral cortex in aging. *Cerebral Cortex*, 14(7), 721–730. <https://doi.org/10.1093/cercor/bhh032>
- Sapnas, K. G., & Zeller, R. A. (2002). Minimizing sample size when using exploratory factor analysis for measurement. *Journal of Nursing Measurement*, 10(2), 135–154.
- Saur, D., Lange, R., Baumgaertner, A., Schraknepper, V., Willmes, K., Rijntjes, M., et al. (2006). Dynamics of language reorganization after stroke. *Brain: a Journal of Neurology*, 129(Pt 6), 1371–1384. <https://doi.org/10.1093/brain/awl090>
- Saur, D., Schelter, B., Schnell, S., Kratochvil, D., Kupper, H., Kellmeyer, P., ... Weiller, C. (2010). Combining functional and anatomical connectivity reveals brain networks for auditory language comprehension. *Neuroimage*, 49(4), 3187–3197. <https://doi.org/10.1016/j.neuroimage.2009.11.009>
- Schwartz, M. F., Saffran, E. M., & Marin, O. S. (1980). The word order problem in agrammatism. I. Comprehension. *Brain and Language*, 10(2), 249–262. [https://doi.org/10.1016/0093-934x\(80\)90055-3](https://doi.org/10.1016/0093-934x(80)90055-3)
- Sullivan, E. V., Zahr, N. M., Rohlfing, T., & Pfefferbaum, A. (2010). Fiber tracking functionally distinct components of the internal capsule. *Neuropsychologia*, 48(14), 4155–4163. <https://doi.org/10.1016/j.neuropsychologia.2010.10.023>
- Suzuki, H., Aoki, K., Chiba, K., Sato, Y., Shiozawa, Y., Shiraishi, Y., ... Ogawa, S. (2015). Mutational landscape and clonal architecture in grade II and III gliomas. *Nature Genetics*, 47(5), 458–468. <https://doi.org/10.1038/ng.3273>
- Tamaoka, K., Sakai, H., Kawahara, J., Miyaoka, Y., Lim, H., & Koizumi, M. (2005). Priority information used for the processing of Japanese sentences: Thematic roles, case particles or grammatical functions? *Journal of Psycholinguistic Research*, 34(3), 281–332. <https://doi.org/10.1007/s10936-005-3641-6>
- Tanaka, K., Kinno, R., Muragaki, Y., Maruyama, T., & Sakai, K. L. (2020). Task-induced functional connectivity of the syntax-related networks for patients with a cortical glioma. *Cerebral Cortex Communications*, 1(1), tga061. <https://doi.org/10.1093/texcom/tga061>
- Tanaka, K., Ohta, S., Kinno, R., & Sakai, K. L. (2017). Activation changes of the left inferior frontal gyrus for the factors of construction and scrambling in a sentence. *Proceedings of Japan Academy Series B Physical and Biological Sciences*, 93(7), 511–522. <https://doi.org/10.2183/pjab.93.031>

- Teichmann, M., Rosso, C., Martini, J. B., Bloch, I., Brugières, P., Duffau, H., ... Bachoud-Lévi, A. C. (2015). A cortical–subcortical syntax pathway linking Broca's area and the striatum. *Human Brain Mapping, 36*(6), 2270–2283.
- Thompson, C. K., & Choy, J. J. (2009). Pronominal resolution and gap filling in agrammatic aphasia: Evidence from eye movements. *Journal of Psycholinguistic Research, 38*(3), 255–283. <https://doi.org/10.1007/s10936-009-9105-7>
- Toro, R., & Burnod, Y. (2005). A morphogenetic model for the development of cortical convolutions. *Cerebral Cortex, 15*(12), 1900–1913. <https://doi.org/10.1093/cercor/bhi068>
- Ura, H. (1999). Checking theory and dative subject constructions in Japanese and Korean. *Journal of East Asian Linguistics, 8*(3), 223–254.
- Walenski, M., Europa, E., Caplan, D., & Thompson, C. K. (2019). Neural networks for sentence comprehension and production: An ALE-based meta-analysis of neuroimaging studies. *Human Brain Mapping, 40*(8), 2275–2304.
- Yeh, F. C. (2020). Shape analysis of the human association pathways. *Neuroimage, 223*, 117329. <https://doi.org/10.1016/j.neuroimage.2020.117329>
- Yeh, F. C., Panesar, S., Fernandes, D., Meola, A., Yoshino, M., Fernandez-Miranda, J. C., ... Verstynen, T. (2018). Population-averaged atlas of the macroscale human structural connectome and its network topology. *Neuroimage, 178*, 57–68. <https://doi.org/10.1016/j.neuroimage.2018.05.027>
- Yeh, F. C., Verstynen, T. D., Wang, Y., Fernandez-Miranda, J. C., & Tseng, W. Y. (2013). Deterministic diffusion fiber tracking improved by quantitative anisotropy. *Plos One, 8*(11), Article e80713. <https://doi.org/10.1371/journal.pone.0080713>
- Yeh, F. C., Wedeen, V. J., & Tseng, W. Y. (2010). Generalized q-sampling imaging. *IEEE Trans Med Imaging, 29*(9), 1626–1635. <https://doi.org/10.1109/TMI.2010.2045126>
- Yotter, R. A., Dahnke, R., Thompson, P. M., & Gaser, C. (2011a). Topological correction of brain surface meshes using spherical harmonics. *Human Brain Mapping, 32*(7), 1109–1124. <https://doi.org/10.1002/hbm.21095>
- Yotter, R. A., Nenadic, I., Ziegler, G., Thompson, P. M., & Gaser, C. (2011b). Local cortical surface complexity maps from spherical harmonic reconstructions. *Neuroimage, 56*(3), 961–973. <https://doi.org/10.1016/j.neuroimage.2011.02.007>
- Yotter, R. A., Thompson, P. M., & Gaser, C. (2011c). Algorithms to improve the reparameterization of spherical mappings of brain surface meshes. *Journal of Neuroimaging: Official Journal of the American Society of Neuroimaging, 21*(2), e134–e147. <https://doi.org/10.1111/j.1552-6569.2010.00484.x>
- Yotter, R. A., Thompson, P. M., Nenadic, I., & Gaser, C. (2010). Estimating local surface complexity maps using spherical harmonic reconstructions. In N. N. Jiang T., J. P. W. Pluim, & M. A. Viergever (Eds.), *Medical image computing and computer-assisted intervention - MICCAI 2007* (pp. 169–176). Berlin: Springer.
- Yuan, T., Zuo, Z., Ying, J., Jin, L., Kang, J., Gui, S., ... Li, C. (2020). Structural and functional alterations in the contralesional medial temporal lobe in glioma patients. *Frontiers in Neuroscience, 14*, 10. <https://doi.org/10.3389/fnins.2020.00010>
- Zhang, N., Xia, M., Qiu, T., Wang, X., Lin, C. p., Guo, Q., et al. (2018). Reorganization of cerebro-cerebellar circuit in patients with left hemispheric gliomas involving language network: A combined structural and resting-state functional MRI study. *Human Brain Mapping, 39*(12), 4802–4819.